universität wien

DIPLOMARBEIT / DIPLOMA THESIS

Titel der Diplomarbeit / Title of the Diploma Thesis

„Printed Macroporous Polymers with Complex Shapes & Structures“

verfasst von / submitted by

Hande Barkan Öztürk

angestrebter akademischer Grad / in partial fulfilment of the requirements for the degree of

Diplom-Ingenieurin (DI)

Wien, 2016 / Vienna, 2016

Studienkennzahl lt. Studienblatt / degree program code as it appears on the student record sheet:	A 066 658
Studienrichtung lt. Studienblatt / degree program as it appears on the student record sheet:	Masterstudium Chemie und Technologie der Materialien UG2002
Betreut von / Supervisor:	Prof. Dr. Alexander Bismarck
Mitbetreut von / Co-Supervisor:	Dr. Angelika Menner

Statutory Declaration

I declare that I have authored this thesis independently, that I have not used other than the declared sources / resources, and that I have explicitly marked all material which has been quoted either literally or by content from the used sources.

Eidesstattliche Erklärung

Ich erkläre hiermit an Eides statt, dass ich die vorliegende Diplomarbeit selbstständig und ohne fremde Hilfe verfasst, andere als die angegebenen Quellen und Hilfsmittel nicht benutzt und die den benutzten Quellen wörtlich und inhaltlich entnommenen Stellen als solche erkenntlich gemacht habe.

Acknowledgment

I would like to express my sincere gratitude and thanks Prof. Dr. Alexander Bismarck, for his brilliant leadership and giving me the opportunity to do this research.

I also wish to thank Dr. Angelika Menner for her assistance and the great help that she provided during my thesis.

I would like to thank to my supervisor, Dr. Qixiang Jiang for his excellent guidance, encouragement and valuable advice during my Master's thesis.

I also would like to acknowledge Claudia Mitterer and Alexander Haubner for their technical support.

I wish to thank Allnex Belgium SA/NV for providing polyurethane diacrylate (PUDA-Ebecryl 8402) samples for the preparing emulsions.

I am thankful to Elisenda Reixach Espaulella and Laia Vilar from Eurocet-CETEMMSA Mataro, Spain for their technical support and for all their help throughout the performing screen-printing.

I am grateful to the MATFLEXEND Research for their financial support.

Finally, I would like to thank my beloved husband, my family and friends for their constant encouragement throughout my master education.

Abstract

REWOD energy harvester has been designed to convert mechanical force into electronic power. In the harvester, a flexible spring element is needed to allow the cyclic wetting and dewetting of the electrodes on the dielectric. The aim of the work is to design the spring elements considering both the formulation side and the processing side.

High internal phase emulsions (HIPEs) with polyurethane diacrylate (PUDA) and 2-ethylhexyl acrylate (EHA) in the continuous phase and with 75% internal phase volume were prepared and UV polymerized. The resulting poly(merised)HIPEs exhibited interconnected and open-porous structure, where the pore sizes were controlled by the agitating speed during the preparation of the emulsions. The polyHIPEs were very flexible, characterized by elastic moduli of between 0.26 and 0.62 MPa and a maximum compressive strain of 75% of their original height. The cyclic loading / unloading tests within the strain range of 10, 20, 40, 50 and 70% of their original height demonstrated that the polyHIPEs can be cyclically compressed and recover. The constant mechanical behaviours of flexible polyHIPEs were shown. Furthermore, dynamic compression tests also demonstrated that the printed prototype of the polyHIPEs can keep the identical mechanical behaviour during a 10 hour test. The flexible and durable mechanical behaviour as well as the open-porous structure of the polyHIPEs made them good candidates for the spring element.

In order to create small and complex shapes, the emulsions were used as ink during the screen printing. The quality of the resulting polyHIPE films, e.g. presence of defects, and the film thickness were highly depended on the viscosity of the emulsions and the mesh sizes of the screens. However, the screen printed films were not high enough to form cage walls in order to use in energy harvester as spring/spacer element. Therefore, emulsions were syringe printed and UV polymerized; polyHIPE cages with desired height were therefore produced. The heights of the cages were controlled by the size of the needles on the syringes during the printing procedure, respectively. REWOD energy harvester prototypes were built to test the function of the polyHIPE spring elements. The capacitance change of the device during the applying and removal of the force indicated the flexible behaviour of the elements.

Zusammenfassung

Der „REWOD Energie Harvester“ ist entworfen worden, um mechanische Kraft in elektrische Energie umzuwandeln. Im „Harvester“ ist ein flexibles Federelement erforderlich welches die zyklische Be- und Entnetzung des Dielektrikum durch die Elektrode ermöglichen muss. Ziel dieser Arbeit ist die Entwicklung dieses Federelementes, sowohl von der Seite der Formulierung als auch von Verarbeitungsseite her.

Es wurden High Internal Phase Emulsions (HIPEs) aus einen wässrigen Innenphasen (75 vol%) und einer kontinuierlichen Phase aus Polyurethan-diacrylat (PUDA) und 2-Ethylhexylacrylat (EHA) hergestellt und UV-polymerisiert. Die resultierenden polymeren polyHIPEs zeigten verbundene und offenporige Strukturen, wobei die Porengrößen über die Rührgeschwindigkeit während der Herstellung der Emulsionen eingestellt wurdet. Der Elastizitätsmodul der sehr flexiblen polyHIPEs lag zwischen 0.26 und 0.62 MPa, bei einer Kompression auf 25% ihrer ursprünglichen Höhe. Untersucht wurden die Rückstelleigenschaften des Federelements in Langzeittests mit 500 zyklischen Kompressionen auf 90, 80, 60, 50 und 30% ihrer ursprünglichen Höhe dabei konnte ein unverändertes mechanisches Verhalten der flexiblen polyHIPE gezeigt werden. Außerdem wurde in anwendungsnahen, dynamischen Druckversuchen gezeigt, dass gedruckte Prototypen der polyHIPEs ein identes mechanisches Verhalten während eines 10-Stunden-Tests halten können. Die Flexibilität und das dauerhafte gute mechanische Verhalten, sowie die offenporige Struktur der polyHIPEs machen sie zu guten Kandidaten für den Einsatz als Federelement.

Um feine und komplexe Strukturen herzustellen, wurden die Emulsionen als Tinte im Siebdruck verwendet. Die Qualität der resultierenden polyHIPE Filme, z.B. Anwesenheit von Defekten und die Filmdicke, waren stark von der Viskosität der Emulsion und von der Maschenweiten des verwendeten Siebes abhängig. Die siebgedruckten Filme hatten jedoch keine ausreichend hohen Käfigwände, die für den Harvester notwendig wären. Über Emulsionen, die mit einer Spritze gedruckt und UV polymerisiert wurden, konnten hingegen polyHIPE-Käfige mit gewünschter Höhe produziert werden. Die Höhe der Käfige konnte durch die Größe der Nadeln auf den Spritzen während des Druckverfahrens gesteuert werden. REWOD-Energie Harvester-Prototypen wurden gebaut, um die Funktion der polyHIPE-Federelemente zu prüfen. Die gemessene Kapazitätsänderung der Prototypen in den Tests beweist die Funktionsfähigkeit der polyHIPEs als Federelement.

List of Symbols and Abbreviations

Symbol	Parameter	Unit
d	Diameter	mm
m	Weight	g
rpm	Revolutions per minute	-
P	Porosity	%
p	Constant of Carreau-Yasuda model	-
s	Constant of Carreau-Yasuda model	-
S	Speed	mm/s
T_g	Glass transition temperature	°C
V	Volume	cm^3
α	Dispense rate	mm^2/s
γ	Shear rate	s^{-1}
γ_c	Critical shear rate	s^{-1}
η	Apparent viscosity	Pa s
η_∞	Newtonian limit viscosity	Pa s
ρ_f	Foam density	gr/cm^3
ρ_m	Skeletal density	gr/cm^3

Abbreviations

ABS	Acrylonitrile butadiene styrene
AIBN	Azobisisobutyronitrile
CAD	Computer aided design
$CaCl_2.2H_2O$	Calcium carbonate-di-hydrate
DMA	Dynamic mechanical analysis
DVB	Divinylbenzene
EDMA	Ethylene dimethacrylate
EHA	2-ethylhexyl acrylate
FDM	Fused deposition modification
HDPE	High density polyethylene
HEMA	Hydroxyethyl methacrylate
HIPEs	High internal phase emulsions
HA	Hydroxyapatite

IBOA	Isobornyl acrylate
IPN	Interpenetrate polymer networks
MBA	N,N′ -methylene bisacrylamide
MIPEs	Medium internal phase emulsions
MPS	Methacryloxypropyltrimethoxysilane
OD	Outer diameter
o/w	oil-in-water
PC	Polycarbonate
PCL	Poly(ε-caprolactone)
PE	Polyethylene
polyHIPE	Polymerized high internal phase emulsions
polyMIPE	Polymerized medium internal phase emulsions
PP	Polypropylene
PUDA	Polyurethane diacrylate
PVA	Poly(vinyl alcohol)
SBS	Poly(styrene-co-butadiene-co-styrene)
SEM	Scanning electron microscopy
SLA	Stereo lithography
SLS	Selective laser sintering
St	Styrene
UV	Ultraviolet
w/o	Water-in-oil
VBC	Vinylbenzyl chloride

Table of Content

1. Introduction

Mobile technologies including smart phones, GPS navigation devices, tablet PCs, are being used increasingly not only for communicating but also accessing the internet, reading a book or as a electronic guide. Aside from the various functions of those devices, the largest advantage is providing mobility to their holders. Therefore, when there is no access to electricity to charge those devices, a portable and easy to use in daily life charger converting other type of energy, e.g. mechanical energy into electrical power, must be designed correspondingly. Krupenkin and Taylor [1] proposed an energy-harvesting device based on converting mechanical energy into electrical energy using Reverse Electro Wetting on Dielectric (REWOD) effect. Therefore, small devices can be charged during walking. The main principle of a REWOD device is that liquid metal droplets or deformable electrodes change their contact area with a dielectric of a charged capacitor, which produces a charge that can be harvested. However, this concept could not yet be integrated into viable devices due to the lack of a spring/spacer element, which keeps the deformable electrodes separated during compression and aids the recovery of the liquid metal droplets after compression to maximize the REWOD effect (Figure 1). Therefore, the motivation of this work is to produce a viable printable spring/spacer element for a REWOD energy harvester.

The spring element should be flexible and durable polymer foams, whose mechanical behaviour can fulfil the requirement for springs under the human walking condition. Consequently, liquid water-in-monomer emulsion templates had to be formulated. These templated had to polymerize fast to result as an elastomeric macroporous polymer. Moreover, the liquid nature of the emulsion templated with a high zero-shear viscosity, should allow them to be used as an ink to process them by printing processes into a micropatterned cage to act as spring element, but simultaneously separate the deformable liquid metal electrodes. Furthermore, to demonstrate the functional spring element, a model REWOD energy harvester prototype was designed, built and tested.

Emulsion templating is a suitable method to produce macroporous polymer with desired morphology and mechanical properties [2]. Therefore the aim of this master thesis was the preparation, processing and application of polyHIPEs in REWOD systems. In this thesis, the following key parts were focused on:

1. The first objective was to prepare emulsion templates to create macroporous monoliths and to investigate the impact of the emulsion preparation conditions, internal phase amount and the adding of SBS on the morphology and mechanical properties of the macroporous polymer monoliths.
2. The emulsion templates of selected flexible and repeatedly deformable macroporous polymers, which were desired for spring element in a REWOD energy harvester, were both screen and syringe printed and the effect of the printing conditions on the resulting macroporous polymer properties were studied.
3. The spring / spacer element was prototyped in order to realise REWOD energy harvester conditions.

2. Theoretical Background

2.1. Reverse electrowetting to energy harvesting

Due to the fast progress in portable and wireless devices, especially sharp increase of the usage of the mobile phones in the daily life, the importance of lengthen power supply to these devices is rising significantly [3]. Therefore, the investigation on producing renewable energy with different methods is the most important part of many research groups. [4][5][6]. One of these researches about energy harvesting is conversion of mechanical energy into electrical energy based on reverse electrowetting phenomenon (REWT). The electrical interaction occurs due to the movement of microscopic liquid droplets between multilayer thin films and from watt to tens of watt energy can be harvested [1].

The working principle of reverse-electro-wetting on dielectric (REWOD) is converting mechanical energy into electric energy by increasing electrically inducing area due to a change in the wetted area on the dielectric surface by the forced liquid droplets (Figure 1a). The choice of non-wetting conducting liquids is limited to high surface tension liquids, such as liquid metals, which form a high enough contact angle on the dielectric. The deforming of the liquid droplets on the electrode by the applied force causes the changing of the effective electrode area during the conversion cycle. At the end of the each completed cycle, the harvested energy, which is proportional to the area increase of the liquid metal, to the dielectric constant k of the separating dielectric and inversely to the dielectric thickness, feeds into an energy buffer. The power density of the harvesters can be as high as 0.1 W cm^{-2} [1].

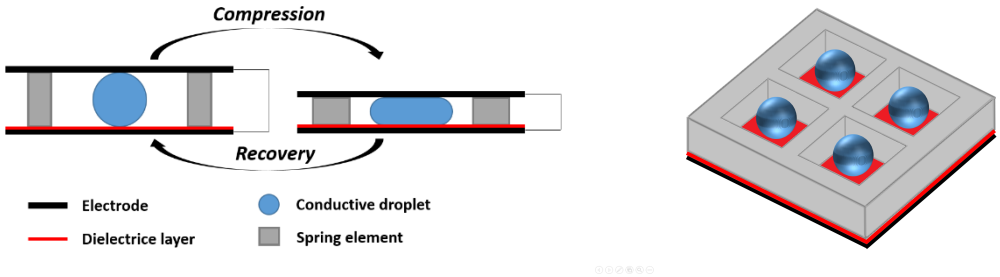

Figure 1: a) Schematic of our REWOD energy harvesting device when compressed (right) and after recovery to its original form (left); b) the spring element is also a micropatterned cage acting as spacer to compartmentalise liquid metal droplets.

In order to achieve reversible-electro-wetting, the electrodes should return original position with the removing of the force on the electrode after the performing of the cycle. Therefore, a flexible and durable spacer between the electrodes can be helpful to returning of the position of the electrode after the removal of the load on the dielectric layers and cause to continue of the wetting-dewetting process. A porous polymer with adjustable mechanical performance and morphology as well as easily processable is a good choice to use as spring element in REWOD device.

Due to REWOD device based on converting mechanical energy into electrical energy, the most common using area to harvest energy is embedding harvesters in footwear [1]. Therefore, during the walking, the electrodes will be compressed cyclically and energy can be harvested based on wetting-dewetting process. Moreover, the harvested energy can be charged many different small devices, including mobile phones and tablets.

2.2. Porous Polymers

Porous materials find a lot of applications in many different areas, from natural porous materials including woods and bones to artificial porous materials such as innovative solutions in high technology industry, including tissue engineering, electric materials, and thermal materials. However, every material containing pores cannot count as porous material. To be a porous material, it should contain lots of pores and those pores should be designed specifically to achieve the expected index of the materials performance [7]. The porous materials can be classified according to number of pores (i.e., porosity), size of pores and into species (i.e., porous metals, porous ceramics and porous polymers). Due to tailored parameters, including designable porosity, high surface area and well-defined morphology, porous polymers have an important place within the group of porous materials [8].

According to IUPAC, porous polymers are characterized by pore size, so microporous polymers as polymeric materials with pore size smaller than 2 nm in diameter, mesoporous polymers with pore size in the range of 2–50 nm, and macroporous polymers with pore size larger than 50 nm [9]. With the smallest pore size, microporous polymers have extremely high surface area and permanent porosity. Due to these different characteristic properties, microporous polymers, which can be synthesized by different techniques including irreversible polymerization reactions, for example by the cross-linking of chloromethylated styrene using Friedel-Crafts alkylation [10], have a variety applications in various fields, such as gas adsorption and storage, catalysis,

light emitting diodes [8][11]. The mesoporous polymers with middle range pore size are synthesized with templates, such as block copolymer templating with inorganic frames [12], reaction-induced phase separation [13] or molecular assembly [14]. Mesoporous polymers can be used as separator of small molecules [15], hydrogen storage [16], tissue engineering [14].

Macroporous polymers, which have 50 nm to 100 μm pore size, have been widely used for industrial applications, e.g. as stationary phase in chromatography, support for catalysts, sensors and adsorbents, as well as biotechnology and biomedicine [17]. They can be produced by, sintering, blowing agents, phase separation, and templating [8]. In order to achieve desired properties of macroporous polymer, synthesize method has great importance. Emulsion templating is an effective way to synthesize polymer foams with tailored properties [18].

2.3. Emulsion templating

Emulsions are heterogeneous mixtures of one immiscible liquid dispersed in another one in the form of droplets. With respect to the dispersed droplets within another liquid phase, the emulsion can be water-in-oil (W/O) or oil-in-water (W/O) [18]. Emulsions can be also classified by the internal phase ratios into high internal phase emulsions (HIPEs, with more than 74.5 vol% internal phase ratio), medium internal phase emulsions (MIPEs, with 30 vol% to 74.5 vol%) and low internal phase emulsions (LIPEs, with less than 30 vol%) [18][19]. Emulsion templating refers to the method exploring emulsions to produce macroporous polymers [20]. The continuous phase of the emulsions contains monomers, while the internal droplet phase serves as a hard template. After the polymerization of continuous phase and the subsequent removal of the internal phase, macroporous polymers are produced. The percentage of porosity of the resultant macroporous polymer is similar to the internal phase volume of the emulsion. Therefore, the morphology of the macroporous polymer can be designed by the emulsion properties and this technique is called emulsion templating [21]. Depending on the use of HIPEs, MIPEs or LIPEs as the templates, the resulting macroporous polymers are named polyHIPEs, polyMIPEs and polyLIPEs, respectively.

PolyHIPEs have been synthesized from HIPEs by free radical polymerization of monomers such as styrene, acrylates and methacrylates [19]. Most of the emulsion templating research is based on the use of styrene (St) and divinylbenzene (DVB) as monomers [22][23] as it is easy to form stable emulsions containing them in the continuous phase and their polyHIPEs possess certain advantageous mechanical properties [23]. However, poly(St-co-DVB)HIPEs are also

characterized by high brittleness and chalkiness, which hinder the potential applications of these polyHIPEs [20]. On the other hand, by using different monomer systems in emulsion templates, the mechanical properties of the resulting polyHIPEs can be tailored, e.g. the brittleness can be reduced. Different stiffness can be achieved by altering the monomers to the acrylate-based elastomers [24]. Cameron and Sherrington [25] investigated to improve mechanical properties of PS/DVB polyHIPE by introducing 2-ethylhexyl acrylate (EHA) to reduce the overall T_g. Hence, the sterically inconvenient styrene-styrene diads were diluted by adding EHA, and thus lend some flexibility to the material. Moreover, Jerenec and co-workers [26] polyHIPE with EHA and glycidyl methacrylate as monomers via emulsion templating; the products were used for chromatographic columns. They found that EHA improves the mechanical stability and reduces brittleness without effecting chromatographic properties.

2.3.1. Preparation of macroporous polymers

HIPEs are highly viscous and paste-like emulsions, but still they are not thermodynamically stable and tend to coalescence. HIPE stability is affected by many different varieties, including the molecular structures of the components comprising the phases and of the surfactant, the surfactant content (5-50 vol.%) [27], the dispersed phase content, the temperature, and the presence of stabilizing salts in the aqueous phase [19].

As an emulsion, HIPEs consist of internal and continuous phases. During the polymerization of the continuous phase of a w/o HIPE, the dispersed droplet of internal phase has turned to pores. Moreover, each droplet has neighbourhood to the other droplet, which transform to pore throats during the polymerization. The volume fraction of the internal phase, the concentration of surfactant and the droplet size are some parameters that affect to the formation of the pore throats [20]. Menner et. al. [28], had focused increasing foam density of polyHIPEs without affecting the interconnected pore network structure. To achieve this, they increased the maximum continuous phase level of HIPEs, which consist of DVB, methacryloxypropyltrimethoxysilane (MPS), non-ionic polymeric surfactant Hypermer 1070 and AIBN from 16% to 40%, and the resultant porous polymers were white and chalky monoliths. Thereby, according to results, the porous polymer with higher mechanical properties was achieved without affecting the highly interconnected nature of the porous medium.

The advantage of emulsion templates is that they can be processed with different methods, including moulding, casting or dispersing in immiscible solvents to produce monoliths [20],

films [29], beads [30] or pattern [24][31]. Monolithic materials can be described as a single piece of continuous porous polymer, which have been fabricated by moulding process and possess an interconnected skeletal pore structure [32]. On the other hand, polyHIPE beads are mostly produced by suspension polymerization of monomer droplets. During sedimentation, individual droplets of monomer solution are partially polymerized through an immiscible sedimentation medium [30]. 2D or 3D ordered user-controlled polyHIPE pattern can be produced with the combination of additive manufacturing techniques and emulsion templating, for example, as scaffold for tissue engineering or porous structure with multi-scale porosity [24].

2.3.2. Fundamental Research into PolyHIPE

Emulsion template polymerization offers the opportunity of widespread use due to many kinetic and technological advantages, such as tuneable mechanical properties and combinability with other techniques, i.e., additive manufacturing [24]. However, water medium causes to the stability problems, because monomers and water phases are very different chemical properties. As a result of changing stability, different kinds of breakdowns occur in the emulsion, which are sedimentation, coalescence, flocculation, phase inversion, creaming and Ostwald ripening [33]. Furthermore, emulsion stability is affected by the droplet sizes of the emulsions, which have dramatic impact on the morphology and, therefore, the properties of porous polymer [21].

The droplets of internal phase have generated the repulsion and it affects the stability of the HIPEs due to kinetic reasons [19]. Aqueous phase can contain salts to enhance the ability of surfactant head groups to pack into an ordered structure by reducing the interaction of non-ionic surfactants with the aqueous phase [34]. Moreover, the salts can also improve stability by inhibiting Ostwald ripening. Several salts can be added into aqueous phase to stabilize HIPEs, including calcium chloride hydrate and potassium sulphate [19].

In order to produce open porous polymer foams, water-in-oil (w/o) HIPEs and MIPEs are commonly stabilized by non-ionic surfactants, which affect the morphology of the resultant macroporous polymer depending on their amount in the emulsion [35]. Surfactant should be completely insoluble in dispersed phase to prevent phase separation and/or phase inversion [19]. Alternatively, stability of the emulsion can be achieved by using particles, which are adsorbed at the interface between the continuous and dispersed phases and form stable particle layer which prevent against droplet coalescence [27]. Particle stabilized emulsions, so-called Pickering emulsions, are stabilized by small particles, such as titania particles [36], bacterial cellulose

nano-fibril [37], carbon nanotubes [27]. In contrast to conventional polyHIPEs produced from surfactant stabilized HIPEs, poly-Pickering-HIPEs have larger but closed-cell pores. Although the interconnected structure of conventional polyHIPE makes them permeable, poly-Pickering-HIPEs made from same monomers and amount of internal phase have better mechanical properties. However, they are usually impermeable, due to the adsorbing of the particles at the oil-water interface of Pickering emulsion droplets and the formation of a closed cell pore wall during polymerisation [38]

Energy input can control pore size and pore throat diameter of the emulsion template. Desirable properties such as high permeability [36], large surface area [39] and mechanical performance [20], can be reached by controlling the morphology of emulsion. Tebboth and co-workers [21] studied controlling gas permeability of macroporous polymers (polyH(M)IPE) by changing energy input during the emulsification. They could show that the average pore size decreased with increasing energy input into the emulsion template, which also tailored the morphological properties. Moreover, very permeable polyH(M)IPE were produced from the emulsion prepared with low energy input, due to low agitation rate causing larger pore and therefore larger pore throats in the resulting porous polymer.

Without any machining, HIPEs can be polymerized in any shape, due to their highly viscous nature [28]. Afterwards the emulsion template is exposed to heat or UV light depending on initiator in order to initiate the polymerization. Initiator can dissolve in both continuous and aqueous phase, and while dissolving of the initiator at the internal phase, polymerization occurs at the interface. On the other hand, the dissolving of the initiator at continuous phase causes to initiate at the same phase. The location of initiation affects the molecular structure, the porous structure and the properties. The research of Livshin and Silverstein [40] indicated that the fast polymerization in the organic phase of w/o emulsion resulted smaller internal phase droplets than the interface-initiation and due to the partial closed-cell structure, resultant organic-phase-initiated polyHIPE has higher moduli than interface-initiated.

2.3.3. Applications of polyHIPE

The range of potential applications of polyHIPEs has broadened due to recent developments in the production of emulsion templated porous polymers. Since highly viscous HIPE can be templated in many different shapes due to particulate stabilizers and ultra-rapid curing by photopolymerization, before sprawling of the emulsion, polyHIPEs can be used in various

advance materials [41]. A large proportion of applications involve using polyHIPEs in fluid separation due to their inherently controllable properties, such as pore morphology, ease of chemical functionalization and high permeability. In the field of fluid separation potential applications are in chromatography, filtration and as membranes [42]. For chromatography applications, polyHIPE can be functionalized [19]. Krajnic et al. [43] studied protein separator-based polyHIPEs prepared with glycidyl methacrylate and ethyleneglycol dimethacrylate monomers via free radical polymerization. After the modification to bear weak-anion exchange groups, the polyHIPEs could separate protein mixture. Another application of polyHIPEs in chromatography has been studied by Martin and co-workers [44]. They prepared acrylamide-based porous polymeric media for protein chromatography, which has dynamic binding capacity for several proteins and it is independent of flow.

PolyHIPEs can also be used as filters for both liquids and gases [42]. In the study of Ikem et al. [45], HIPEs stabilized by oleic acid-modified silica particles were polymerized to use as an alternative to gravel packing, which is a well-known technique for sand control in horizontal oil wells. Another study for separation of gases was performed by Muchan et al. [46] They prepared the porous polymer from HIPE contained VBC and DVB monomers in the continuous phase and functionalization of polyHIPE was made with amine for CO_2 adsorption. The adsorption was achieved, but it is depend on the type of amine group.

Due to the liquid form of HIPEs, they can be templated into an appropriate mould before polymerization to produce monoliths or membranes. [42]. In the study of Pulko and co-workers [29], HIPE was prepared with glycidyl methacrylate, ethyleneglycol dimethacrylate and 2-ethylhexyl methacrylate (EHA) monomers and casted onto glass substrate to polymerize. The percentage of EHA and ethyleneglycol dimethacrylate influenced the flexibility and morphology of the resulting membranes. After the porous membrane was functionalized with diethylamine, ion exchange chromatographer was achieved.

The high porosity and good mechanical property of polyHIPEs make that excellent candidate as matrixes for tissue engineering. However, in order to introduce polyHIPEs into biologic environment, the porous polymers should be hydrophilic and have enough water absorption [41]. To enhance water absorption, 2-Hydroxyethyl methacrylate (HEMA) based polyHIPEs have been investigated by Kulygin and Silverstein [47]. In this research, HEMA was polymerized with methylene bisacrylamide (MBAM) crosslinker via thermal polymerization of oil-in-water

(o/w) HIPE. Increasing MBAM amount caused also increasing surface area and water absorption, which are important parameters for tissue engineering applications. On the other hand, biodegradability is important factor for some tissue engineering areas. Lumesky and co-workers [48] was achieved biodegradable open-pore polyHIPE with copolymerization of biodegradable polycaprolactone (PCL) oligomer with PCL-VL or formation of a semi-IPN with PCL oligomer. They found that the semi-IPN contained large voids, which can be more suitable for biodegradable tissue engineering applications than the typical polyHIPE structure.

Furthermore, polyHIPE can also be used to absorb and transport liquids. Shkolnikov and co-workers [49] studied on polyHIPEs to use as wick, which is an integral part of fluid capacitance and transport area, such as heat pipes, vapour chambers, microfluidic systems, fuel cells and electrospray nozzles. They produced porous monoliths of 2-hydroxyethyl methacrylate-co-ethylene dimethacrylate (HEMA-co-EDMA) via free radical, UV-initiated polymerization. The designed polyHIPE were highly permeable, hydrophobic, dimensionally and chemically stable and most importantly fabricated on an aluminium cathode to use as wick.

Besides all these application areas, polyHIPE can be produced with the combination of additive manufacturing and emulsion templating. Due to exploration of subsequent use of UV light to cure the HIPEs, it is now possible to create polyHIPEs with defined 3D architectures [24][31][50].

2.4. Printing technology

Printing is an advanced method to make thin films, in which the ink is spread into thin layers; a pattern can be applied simultaneously. After centuries, the application areas of printing have been extended from publishing and art to engineering applications, such as bioengineering, preparation of electric devices [51][52][53] and solar cells [54][55][56] using gravure printing, screen printing and inkjet printing. Besides all these printing techniques, additive manufacturing technique are being recently employed in academic laboratories and industry for various applications from electronic devices to medicine [57][58][59]. Screen and 3D printing will have been explained detail.

2.4.1. Screen Printing

Screen printing is a stencil process including closed non-image areas and open image areas and this process works by forcing the ink through a screen by a squeegee (Figure 2) [60]. The screen-

printing technique is fast, low cost and adaptable. Because of the advantages of the fabrication process it has been used to manufacture conductors, resistors, and dielectrics since the mid-1960s [61].

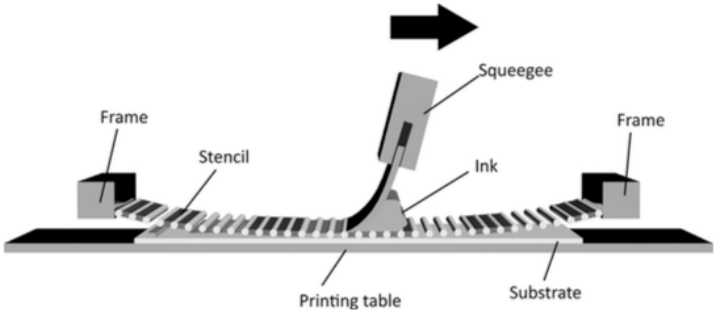

Figure 2: Screen printing process [60].

Accurate results with many different parameters are obtained by using screen printer machines. To reach desired products, the combinations of variables such as distance between the screen and the substrate, mesh size, and squeegee parameters, including the printing speed, pressure, geometry, angle and softness need to be arranged. After the parameters of squeegee are set, the ink is placed on the screen, before the squeegee, and by starting the squeegee presses the ink onto the substrate through the screen. After the squeegee movement, the substrate and screen separate. The material of the screen can be stainless steel or polymer. There are two main techniques of screen-printing [62]:

- Off-contact, while tension was applied direction of the substrate, the screen is bended;
- Contact, the screen is in full contact with the substrate. Therefore, damage can happened during the printing of high resolution.

The largest effect on the film quality for the same emulsions is the open areas on the fabric, which corresponds to the number of threads/cm and the threat thickness in μm. The fabrics having between 40 and 120 threads/cm are the most frequently used, while better print quality can be obtained from fabrics with higher threads/cm [60]. The open areas of the fabric decrease with increasing thread number per centimetre for the screens having the same thread thickness. Therefore, the thinner ink should be chosen while a screen with large thread count such as 145T was used [63].

Keeping the same printing conditions over the whole area is one of the biggest challenges. To ensure the same patterns throughout the panel, the off-contact speed should be maintained

steady. The other factors affecting the printing quality are distance between screen and plate and viscosity of the ink [64].

2.4.2. 3D Printing

3D printing is an additive manufacturing technique. This method based on printing a layer of liquid material and followed by immediate solidification of the layer, and then a second layer can be built on top of the previous printed ones. Eventually, stacking of layers leads to a 3D shape. Even though 3D printing currently is used to build and design prototypes and small objectives, due to performability of processing into any shape or geometry from a 3D model source, many research groups and different types of industries have focused on developing this method into a versatile future production method [58].

Depending on fabrication principles, the 3D printing process can be classified: (1) Fused Deposition Manufacturing, (2) Stereo Lithography, and (3) Selective Laser Sintering [58][65]. Fused Deposition Manufacturing (FDM) is the most flexible, low cost and popular printing method (Figure 3). Generally, the raw material includes wires, rolls, laminates and pellets are molten and extruded out from the nozzle, while the nozzle is moving to pattern the 3D patterns. The extruded molten cools down and therefore solidify immediately. Thermoplastic polymers have been used, such as acrylonitrile butadiene (ABS) [66], polycarbonate (PC) and high density polyethylene (HDPE) [58]. Moreover, some polymers are made composite powder of poly(vinyl)alcohol (PVA) with hydroxyapatite (HA) to print scaffold [59] or loaded model drug, such as synthetic corticosteroid Budesonide [67], fluorescein [68] into PVA.

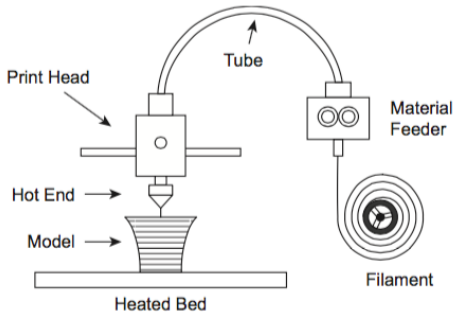

Figure 3: Illustration of the working principle of FDM-based 3-D printing [58].

The 3D printer using in this research is based on FDM. However, during the printing process with FDM, thermoplastic polymers are used, after they melted into the hot part of the printer head. Conversely, the hot area is not necessary during the printing of macroporous polymer

shapes, because of the liquid formation of HIPEs. Therefore, FDM was modified with dispenser, which will help to inject HIPE with desired amount and this system is called syringe printer.

Stereo lithography (SLA) method produces a design layer-by-layer using photopolymerization from liquid monomers and resins (Figure 4). With the help of computer aided design software, during the designing of the photopolymer resin, the UV light cure the shape and resin is solidified. This process is repeated for each layer. The biggest disadvantage of SL against FDM is high cost of resin. On the other hand, it is a fast process [58]. SLA can be applied in tissue engineering, such as using epoxy/hydroxyapatite UV curable suspension [69], biodegradable resin [70] or poly(d,l-lactide)-based resin [71]. Moreover, SLA is used for electronics fabrication [72], ceramic suspensions [73][74], porous polymers [75] and many others.

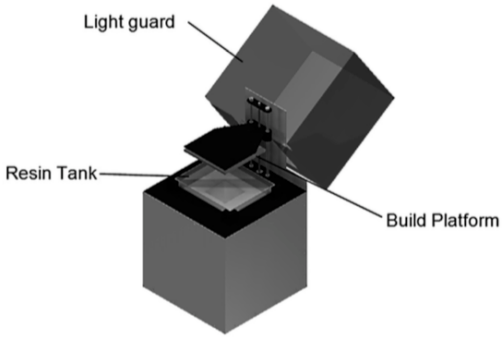

Figure 4: Principle of how SLA 3-D printing works [58].

Selective Laser Sintering (SLS) method creates complex 3D parts based on consolidating layers of powder material on top of each other (Figure 5). Laser beam consolidate the selected area, which has been calculated by CAD (computer-aided design) model and scanned [76].

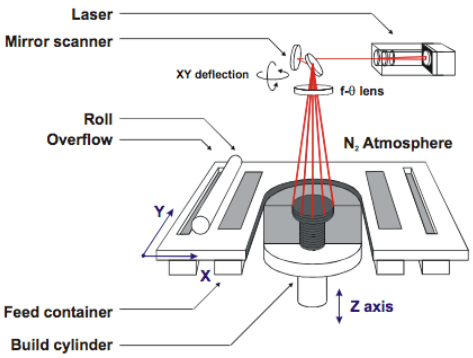

Figure 5: A typical SLS machine layout [76].

3. Experiment

3.1. Materials

2-ethylhexyl acrylate (EHA), $CaCl_2.2H_2O$ were purchased from Sigma-Aldrich (Vienna, Austria). Polyurethane diacrylate (PUDA, Ebecryl 8402) was kindly supplied by Allnex Belgium (Brussels, Belgium). SBS D 1102 AU were kindly supplied by Kraton (Amsterdam, Holland). Hypermer B246, supplied by Croda (East Yorkshire, UK), was used as surfactant. Darocur 1173, purchased from Ciba (Basel, Swaziland) was used as UV initiator. All the monomers were used as received.

3.2. Emulsion preparation

Emulsion template was prepared in a reaction vessel equipped with a glass paddle rod connected to an overhead stirrer. The internal phase of emulsion was aqueous solution of 10g/L $CaCl_2.H_2O$. EHA, PUDA, initiator, surfactant and, in some cases, SBS were mixed in the vessel. The internal phase was dropped into the continuous phase under stirring at speed of 400 rpm. Afterwards, the emulsions were further stirred at different speeds for 90 seconds to homogenize the emulsions. Five emulsion templates were prepared and the detailed recipes are summarized in Table 1.

Table 1: Formulations of acrylate-based emulsions.

	H1	**H2**	**H3**	**M1**	**M2**
Continuous phase (vol%)[1]	25	25	25	35	35
EHA (vol.%)[2]	58.8	58.8	58.8	58.8	55.4
PUDA (vol.%)[2]	35.3	35.3	35.3	35.3	33.2
Hypermer B246 (vol.%)[3]	5.9	5.9	5.9	5.9	5.9
Darocur 1173 (Mol%)[4]	2	2	2	2	2
SBS (vol.%)[2]	-	-	-	-	3.3
Internal phase (vol.%)[5]	75	75	75	65	65
Stirring speed (rpm)[6]	600	1000	2000	2000	1000

[1] The continuous phase volume ratio is with respect to the entire volume of emulsion.

[2] The monomers volume ratio is with respect to the continuous phase volume.

[3] Surfactant ratio is with respect to the continuous phase volume.

[4] Initiator ratio is molar percentage of the amount of carbon-carbon double bonds in the monomers.

[5] The internal phase volume ratio is with respect to the entire volume of emulsion.

[6] Stirring speed is after the finishing of dropping of the internal phase.

3.3. Macroporous polymer preparation

3.3.1. PolyHIPE monoliths mould preparation

The emulsions were placed into a mould with an inner diameter of 10 cm and a height of 7 mm and the upper surface was flattened with a ruler. Then, the emulsion in the mould was polymerized 14 minutes under an UV light (Light Curing Conveyor Systems UVC-8, DYMAX, Wiesbaden, Germany). Afterwards, the monolith was demoulded and dried in oven at 50 °C for 24 hours to remove the internal phase.

3.3.2. Screen printing of emulsion templates

The four different emulsion templates (H1, H3, M1 and M2) were employed as inks in screen printing experiments using a Digital Electric Flat Screen Printer (AT-GOLD, ATMA, Taiwan). Therefore, five screens, namely 34T, 62T, 77T, 120T polyester screens and A-200 steel screen, with different mesh sizes were used. Mesh size is measured by how many threads of mesh per centimetre [60]. The PP substrate was placed on the surface of the screen printer, during the printing with lowest speed, which is 125 mm/s, the distance between the screen and the substrate was changed from 3 mm to 5 mm and 7 mm in order to investigate the effect of the height of the screen from the substrate on the film thickness. The steel blade spread the ink firstly on the screen. Then the squeegee pressed down the screen to contact substrates, while its angle is 75° against the screen. The squeegee spreads and pushes the inks through the screen at a speed of 125, 250, 400 and 600 mm/s, respectively. After that, the printed emulsion on the substrate was placed in a water bath, polymerized 2 min using a UV light (Curing Flood System 2000PC, DYMAX, USA) and afterwards dried at the room temperature.

3.3.3. Syringe printing of emulsion templates

The syringe printing set-up consisted of Stepcraft 420 Construction Kit (Iserlohn, Germany) and dispenser (Ultimus IV Positive displacement dispenser, Nordson

Corporation, Bedfordshire, UK). After emulsion was transferred into the syringe from the vessel, the needle was attached to the syringe. The cage patterns were printed with two needles with different diameter (0.5 mm and 0.7 mm) to investigate the effect of outer diameter of the needles on the wall dimensions. The syringe was placed into movable head of printer system and its plunger was connected to the dispenser. The distance between the needle and the substrate was equal to the outer diameter of the needle. The dispensing of the ink was driven by the dispenser while the syringe was moving following pattern via computer software on the substrate. The printed emulsion was polymerized in the water bath and, afterwards, dried in the oven at 50 °C.

3.4. Characterization

3.4.1. Rheological test

Rheological measurements of HIPEs and MIPEs were carried out using Discovery Hybrid Rheometer HR-3 (TA Instrument, Eschborn, Germany) with cone-cup geometry at 25 °C. The gap between rotor and cylinder is 0.52 mm. When shear rate sweep is between 10^{-6} and 100 s^{-1}, rheological behaviours were measured, which determines if properties are changing over the flow.

3.4.2. Morphology of the polyH(M)IPEs

The morphology of the macroporous polymers was observed using scanning electron microscopy (SEM, JCM-6000 Neoscope Benchtop SEM by Jeol, Germany). The moulded and cut as with dimensions of 15 mm by 15 mm and height of 7 mm samples were separated without using any cutter and the separated sides of the monoliths were gold-coated for SEM to obtain sufficient conductivity prior to observation (Jeol, JPC-1200, Fine Coater, Germany). The 60 different pore and pore throats of the images were measured using software ImageJ open source image processing program.

3.4.3. Densities and Porosities

The skeletal densities of the macroporous polymers were measured using helium pycnometer (Accupyc 1330, Micrometrics Ltd., Limited, Dunstable, UK). The samples were cut into small pieces. Approximately 0.13 gr of each sample was filled into 1 cm^3 chamber and weighed. Helium was charged into the chamber with the samples until a pressure of 0.131 MPa was reached. Then the volume of the material

was determined by the difference of the volume of the empty chamber and the chamber with the samples, thus the density of the material could be calculated. To measure the foam densities, the polyH(M)IPE monoliths were cut into cubic specimens with dimensions of 15 mm by 15 mm and height of 7 mm; the specimens were weighed and the foam densities (ρ_f) were calculated by:

$$\rho_f = \frac{m}{V} \quad \text{(Eq. 1)}$$

Where, m is the weight of the sample and V is the volume of the sample.

The porosities, *P*, of the samples were calculated by:

$$P\,(\%) = \left(1 - \frac{\rho_f}{\rho_m}\right) * 100 \quad \text{(Eq.2)}$$

Where, ρ_m is the skeletal density.

3.4.4. Mechanical Tests

3.4.4.1. Compression test

The compression tests were carried out at room temperature using the Instron series 5584 testing machine (Instron Ltd., Norwoord, U.K.) equipped with a 1 kN load cell. The specimens were with dimensions of 15 mm by 15 mm and height of 7 mm. The samples were compressed at an extension rate of 1 mm/min until the height was reduced by 75% of its original value. Elastic modulus was determined from the slope of the initial linear elastic region in the stress/strain plot. The crush strength was determined from the maximum compressive strength of the sample at the end of the initial linear elastic region, normalized with respect to the cross-sectional area.

3.4.4.2. Cyclic compression test

The cyclic compression tests were performed. The polyH(M)IPE specimens were cut same way with the sample of the compression test, were measured at room temperature using Instron series 5584 testing machine (Instron Ltd., Norwoord, U.K.) equipped with a 1 kN load cell at an extension rate of 5 mm/min. The samples were compressed until the thickness was reduced by 10%, 20%, 40%, 50% and 70% of their original height, respectively, and unloaded for 500 times. Then, the viscoelastic deformations of the samples were calculated from the strain value of the cross-section to zero of stress value of released line at the 500^{th} cycle.

3.4.4.3. Cyclic compression test using Dynamic Mechanical Analysis (DMA)

Dynamic compression test were carried out using DMA (RSA-G2, TA Instruments, USA). After the H3 and M2 recipes were printed with syringe printer, the cages were cut into 1 cm^2 area including 9 cages, and compressed to 30% of its original value at a frequency 2 Hz for 10 hours. The changing of storage modulus was evaluated versus time.

3.4.5. Energy harvesting test

In order to investigate the capacitance change due to the applying force to the spring element with metal droplets, H3 and M2 emulsions were patterned as cage shapes via syringe printer connected 0.7 mm outer diameter needle on Mylar® Dielectric coated cupper plates (kindly supported by IZM, Fraunhofer, Berlin, Germany) and 16 Hg droplets were placed into the cages, of which the total area were approximately 1.1 cm^2, to measure the capacitance change against pressure. The heights of the Hg droplets were close to the height of the cell walls. Another copper plate was placed on top of the cages and droplets. The capacitance changes of the system before and after added 10 N/cm^2 force on the cupper layer was measured via VOLTCRAFT VC940 voltammeter (digital multimeter, Conrad, Vienna, Austria).

4. Results and discussion

4.1. Macroporous polymer monoliths

The pore and pore throat diameters and porosity are the main parameters that affect the mechanical properties of polyH(M)IPE, which have same monomer content [21]. Therefore, the energy input during emulsification, i.e. the stirring rate, and the internal phase amounts, which are 65 % and 75 %, were varied in order to investigate their influence on the pore size and porosity. Moreover, the effect of adding SBS to MIPE was also studied. Table 1 summarises the formulations of all the samples. All produced polyH(M)IPEs have open porous structure, characterized by spherical pores, which were templated from the droplets in the original emulsions and pore throats, which formed during the polymerization of emulsion templates (Figure 6).

4.1.1. Morphological behaviours of macroporous polymer monoliths

The skeletal density of all polyH(M)IPEs were identical, as they were produced from the same of monomer content, which are PUHA and EHA. Even though PM2 has minor amount of SBS content, it did not affect the skeletal density. The porosity of the polyHIPEs are 73%; since the polyHIPEs were templated from the emulsions with internal phase of 75%, the porosity of the resulting polyHIPEs is expected to be in the same range as the internal phase ratios. Furthermore, the foam density and the porosities of PM1 and PM2 are similar, because they were templated from the emulsions with internal phase of 65% but M2 has also SBS content (Table 2).

Table 2: Pore sizes, pore throat sizes, densities, and porosities of polyH(M)IPEs.

	Porosity (%)	**Skeletal density (g/cm^3)**	**Foam density (g/cm^3)**	**Pore size (µm)**	**Pore throat size (µm)**
PH1	74 ± 1	1.1 ± 0.01	0.3 ± 0.01	8 ± 3	1.6 ± 0.6
PH2	73 ± 1	1.1 ± 0.01	0.3 ± 0.01	6 ± 2	1.4 ± 0.5
PH3	73 ± 2	1.1 ± 0.02	0.3 ± 0.01	3 ± 1	0.6 ± 0.3
PM1	62 ± 2	1.1 ± 0.01	0.4 ± 0.01	3 ± 1	0.9 ± 0.3
PM2	65 ± 1	1.1 ± 0.01	0.4 ± 0.01	4 ± 1	1.5 ± 0.5

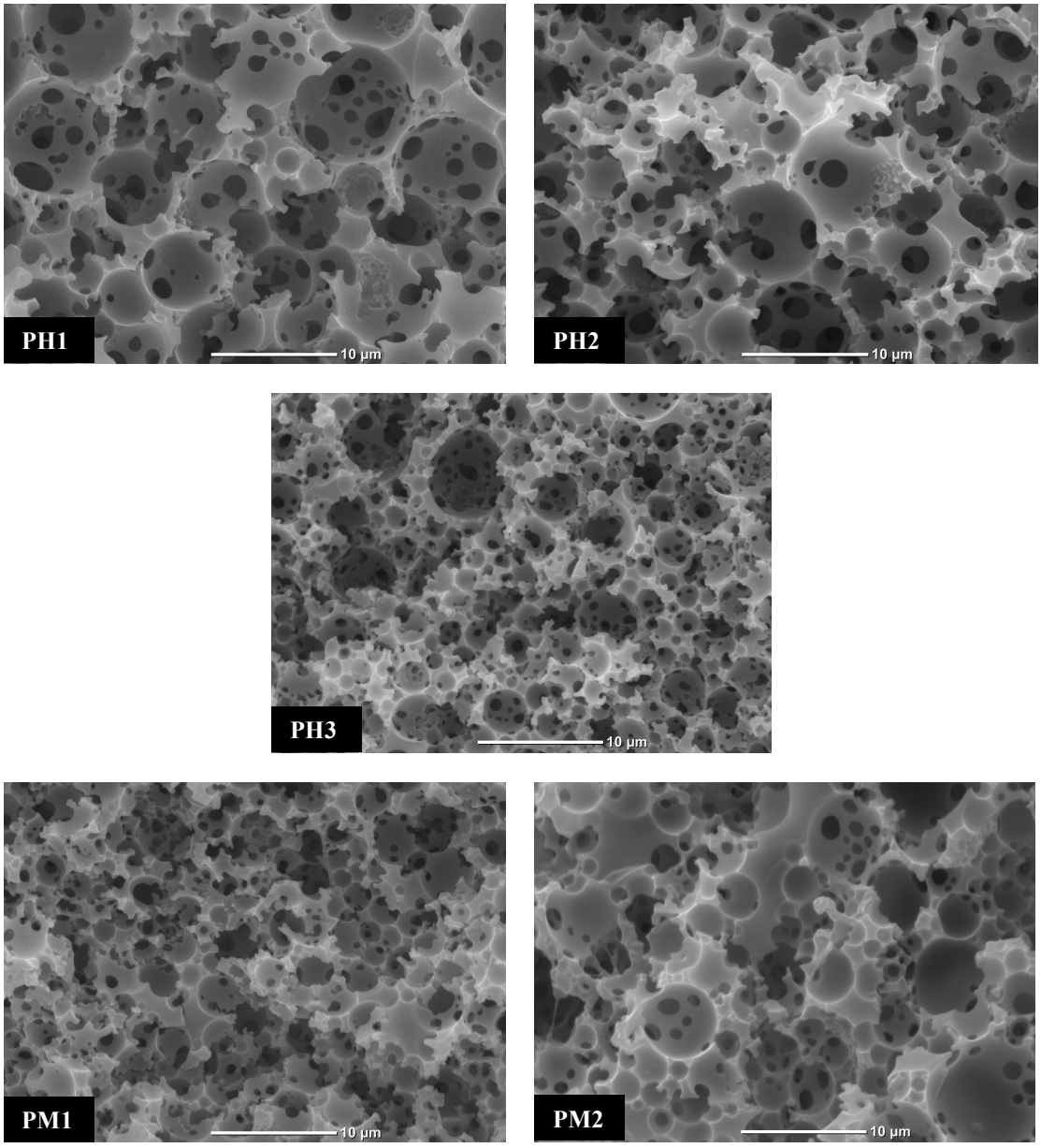

Figure 6: SEM images of polyH(M)IPE samples.

PolyHIPEs PH1-PH3 have an open-porous structures, which was as expected as they were produced using surfactant-stabilized-emulsions [77][38]. The pore sizes of the PH1-PH3 reduced from 8.4 µm to 2.8 µm (Table 2 and Figure 6), indicating that the droplet sizes within the emulsion templates of H2 and H3 were reduced compared to H1. During the emulsification of HIPEs, while the agitation rate was 600 rpm for H1, H2 was prepared with 1000 rpm and H3 with 2000 rpm. The higher energy input promoted the higher shearing of the internal phase and, therefore, its break up into smaller droplets, which subsequently led to smaller pore sizes after the polymerization [78]. Furthermore, the pore throat sizes of PH1 to PH3 reduced from 1.6 µm to 0.6 µm. The pore throats formed due to mechanical rapture of the

polymeric walls between the neighbouring droplets in the emulsions during the polymerization [79]. The raptured area of two small droplets must be small. Therefore, after the polymerization, the PH3 with smaller pores possessed smaller pore throats compared to PH1 and PH2. Skeletal densities of the polyH(M)IPEs were measured by pycnometer from the granulated macroporous polymer monoliths. On the other hand, calliper was used to measure the dimensions and calculate the volumes and foam densities of the sample, because using another pycnometer method to measure the foam density of the porous polymer, such as Geopyc 1360 (Micrometrics Ltd., Limited, Dunstable, UK) which is usually used in our group, can deform the sample significantly, due to the flexibility of the acrylate based polyH(M)IPE and cause systematic error. The foam densities of PH1-PH3 increased gradually, corresponding to the slight decrease of their porosities (Table 2).

Due to the stabilization of MIPEs with surfactant same as HIPEs, PM1 and PM2 had also open-porous structure (Figure 6). The pore sizes of the polyMIPEs increased from 3.2 µm to 4.4 µm, respectively as a result of increasing droplet size within the emulsion templates; the energy input affects the MIPEs and, therefore, the polyMIPEs in the same way as the HIPEs and polyHIPEs. However, this increase in the pore size was not as sharp as the change between PH2 and PH3, due to the SBS content in the PM2. Moreover, pore throat sizes of PM1 to PM2 raised from 0.9 µm to 1.5 µm, due to the increased the pore sizes. PM1 and PM2 had higher foam densities than polyHIPEs, because they were templated from 65 vol.% internal phases and the porosity affects the foam density. On the other hand, the minor amount of SBS content in PM2 led to a decreased the foam density (Table 2).

4.1.2. Mechanical behaviours of macroporous polymer monoliths

4.1.2.1. Compression test

Since the polyH(M)IPEs shall be used as spring elements, the compressive properties were characterized. Figure 7 shows the compression stress-strain curves of all macroporous polymer monoliths; the results are summarized in Table 3. When the samples were compressed by 75% of their original height, a similar trend can be observed for all the samples in the stress-strain curves. The samples underwent elastic deformation, from which the elastic moduli were calculated. The elastic moduli of polyHIPEs are with about 0.26 MPa identical within errors, as they were produced

from HIPEs having the same monomer compositions and same internal phase ratio, namely 75%, but produced with different agitation rates (Table 1). The elastic modulus of PM1 (contains SBS (Table 1)) and PM2, which were produced from the 65 vol.% internal phase emulsions, which were stirred at different agitation rates are with 0.62 MPa and 0.55 MPa, respectively higher than those of the polyHIPE samples (Table 3). The compositional changes and morphology affect the mechanical performance of flexible macroporous polymers. Therefore, polyHIPEs with higher porosity than polyMIPEs have the lower elastic moduli. These results are consistent with the previous findings [20][25]. Moreover, the elastic modulus of PM1 is higher than PM2 due to both the SBS content in the PM2 and also lower pore and pore throat diameter of PM1.

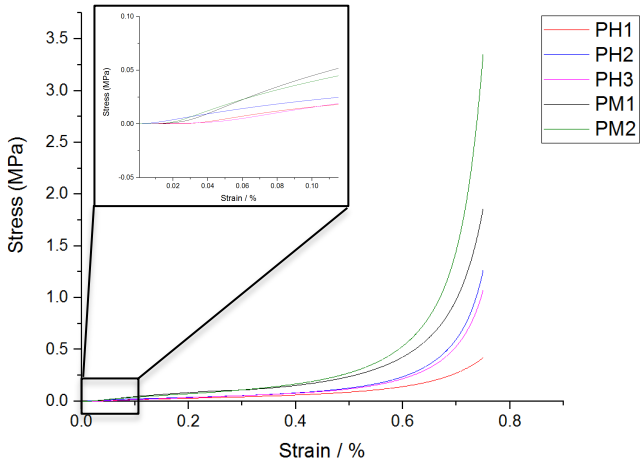

Figure 7: Exemplar stress-strain curves of the various polymer foam materials under compressive load.

Table 3: Mechanical properties of polymer foams.

Sample name	Elastic Modulus (MPa)	Crush Strength (MPa)
PH1	0.3 ± 0.01	0.06 ± 0.01
PH2	0.3 ± 0.01	0.06 ± 0.01
PH3	0.3 ± 0.01	0.09 ± 0.01
PM1	0.6 ± 0.04	0.13 ± 0.01
PM2	0.5 ± 0.04	0.13 ± 0.01

After the initial linear, elastic region, the stress-strain curves entered the second linear region rather than a stress decrease after a compressive strain of about 10% of their original height. This suggests the samples did yield but did not fail during the compression test. As a result of that crush strength exist for macroporous polymer monoliths. The crush strengths of the samples were determined from the maximum strength at the end of the initial linear elastic region of the stress-strain curves. While

the crush strength of PH1 and PH2 were 0.06 MPa and identical within the error, the crush strength of PH3 was 0.09 MPa (Table 3). Since the monomer compositions in the HIPEs were same, the improvement of the mechanical properties of the polyHIPEs might be attributed to the decrease in pore and pore throat size of PH3. On the other hand, the crush strength of PM1 and PM2 were 0.13 MPa identical within the error (Table 3). In recent years, SBS is used to modify bitumen for a better performance by increasing the elasticity in both asphalt cements and mixtures [80] and also as shock absorber in shoes soles [81]. Thus, when the elastic modulus of PM2 is less than the elastic modulus of PM1 due to the changing morphology of polyMIPEs, i.e., increasing pore and pore throat diameter of PM2, the crush strength of PM2 should also decreased but, surprisingly, they were identical.

At a compressive strain of about 50% of their original height, the samples entered the densification stage, where the stress accumulated significantly without a great increase in the strain [20][27]. Once the polyH(M)IPEs will be used as the spring elements, the densification presents the overload of the spring. Therefore, the beginning of the densification strain indicates the upper limit of the strain for the sample being used as springs. Consequently, the macroporous polymer monoliths can be used below the 50% compressive strain rate of their original height without changing their mechanical properties.

However, the criteria of the stress during human walking is $9N/cm^2$, which equals 0.09 MPa [82]. Therefore, the crush strengths of PH3, PM1 and PM2 are in the range of the applying stress during the human walking. That makes them good candidate for spring element.

4.1.2.2. Cyclic Compression test

Since the polyH(M)IPE are intended to be employed as spring elements in REWOD energy harvester, the candidate materials for the spring / spacer element will have to deform reversibly. Therefore, the polyH(M)IPE were subjected to cyclic compression testing. In order to investigate the durability, the macroporous polymer monoliths were deformed for 500 cycles by up to 10, 20, 40, 50 and 70% of their original height, respectively.

Cyclic compression test for 50% strain rate of PH2 and PM2 are shown in Figure 8 to indicate that the samples underwent the densification after 50% strain rate, which

represents the overloading of the springs. However, the stress-strain curves follow identical loops without any significant deformation (The rest curves are in Appendix I and II). The corresponding compressive stress were higher than the restoring stress of the unloading curves, due to the occurring of hysteresis as a result of the viscoelastic behaviour of the polymer chains [83], which is typical for rubbery polymers. The stress-strain loop from the loading and unloading decreased significantly in the first several cycles, but after the 10th cycle, the material response was very reproducible (Figure 8). As a result of stress-softening, the downwards shifting of the stress-strain loop occurred cycle by cycle, which has been known as the Mullins softening effect of elastomers [84].

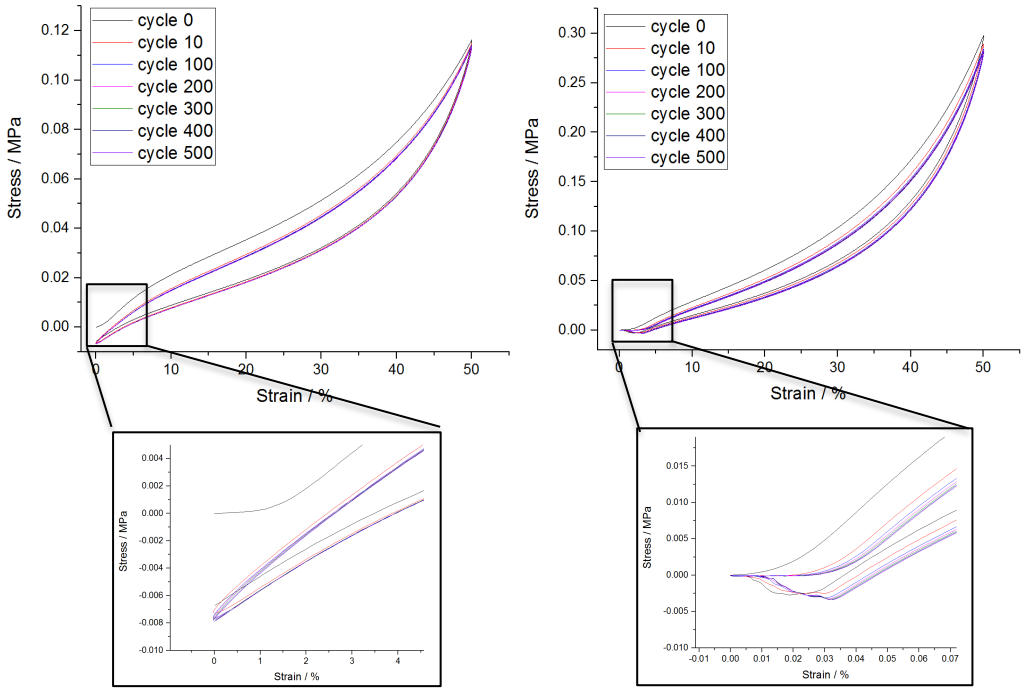

Figure 8: Cyclic compression test for 50% strain rate of PH2 (left) and PM2 (right) monoliths.

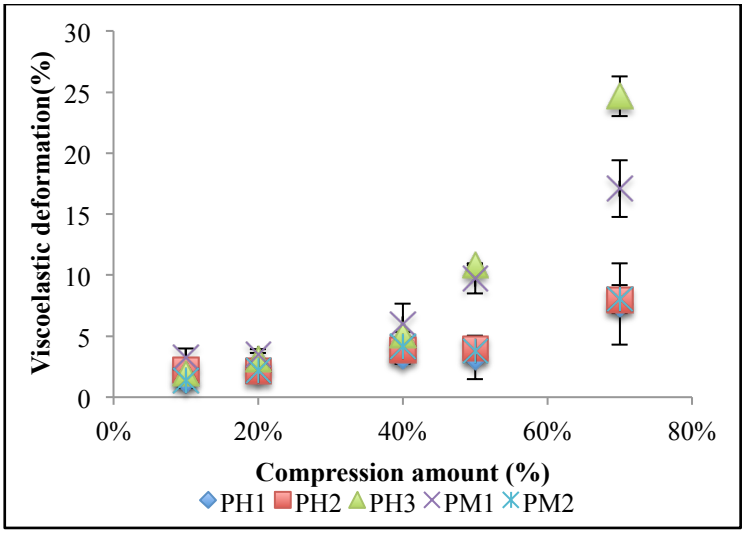

Figure 9: Viscoelasticity of porous polymer samples at different compression amounts.

Although the loading-unloading curves reach a constant compressive stress after 10th cycles, the strain did not recover completely during unloading. The deformations of the samples were permanent within the time frame of the measurement. However, the samples regained their original height within 24 hours, which indicates that deformation is viscoelastic. Due to the softening of polyH(M)IPEs, they loose their height as equal to the viscoelastic deformation of the monolith. Therefore, the reading on the stress was zero but there was still strain remaining. The residual strain for all the samples increased with the cyclic compression strains, the increase became more significantly when the strain of the samples was beyond 50% (Figure 9)(Appendix II). During the human walking, approximately 0.1 MPa compressive stress was expected [82] and it is roughly equal to the 30% strain rate, which is lower than densification strain rate of macroporous polymer monoliths. Therefore, it is safe to use the materials in 30% strain rate range.

PH1 and PH2 had similar viscoelastic deformation for all compression strain rates (Figure 9), due to the same porosity and close pore and pore throat diameters (Table 2). However, even though the viscoelastic deformation of PH3 was near to the viscoelastic deformation of PH1 and PH2 for 10, 20 and 40% strain rates, the value increased sharply after 50% strain rate (Figure 9)(Appendix I). Since the recovery of viscoelastic polymers mostly relates with the gas permeability, the decrease in the pore throat size affects the viscoelastic deformation of polyH(M)IPE. Therefore, PH3 with the lowest pore throat sizes (Table 2) had limited air refilling between cycles and large deformation for 50% and 70% strain rates of its original height occurred.

The viscoelastic deformations of PM1 were higher than polyHIPEs for all compressive strain rates as expected (Figure 9), because it had the highest elastic modulus and crush strength then other monoliths due to low porosity and high foam density, but the high elastic modulus limits also recovery of the sample (Table 3). Moreover, the small pore throat size of PM1 also affected the higher viscoelastic deformation compare to PH1, PH2 and PM2 (Table 2). On the other hand, PM2 with 65% porosity has higher elastic modulus and crush strength than polyHIPEs; but its viscoelastic deformation is similar to PH1 and PH2, which had 75% porosity and lower elastic deformation than PM2 (Table 2) (Figure 9). The reason of that is that the pore throat diameter of PM2 is similar to that of PH2, of which were higher than the pore throat diameter of PH3 and PM1. Moreover, the minor amount of SBS content in PM2 improves the flexibility of polyMIPE (Figure 9)(Appendix II). It has been known that SBS soften even rigid polymer matrixes and stop the growing crazes [85].

4.2. Printing emulsion templates

4.2.1. The rheological behaviours of M/HIPEs

Due to the liquid nature of the emulsions, they can be used as inks and printed to create films and cage patterns. Rheological behaviour of printing emulsions have direct impact on the quality of printing. A rheometer was used to determine the flow properties and behaviours of materials processable in fluid form [86]. Relative motion between each molecules and internal friction forces exhibit during flowing cause a resistance to flow, which is described by viscosity and it is also related to the shear rate [87]. During the screen printing, the emulsion are exposed of various shear rates, which occur as a result of spreading the emulsion with blade, pressure of the squeegee, penetrating the emulsion to screen mesh. According to Lin and co-workers [86], the maximum shear rate for ordinary printing screens may reach 1000 s^{-1}.

The rheological properties of HIPEs and MIPEs listed in Table 1 were investigated on the shear-dependent viscosity behaviour (Figure 10). All emulsions showed a bent to reach the zero-shear viscosity η_0 at very low shear rates and act like a Newtonian system, which viscosity is independent of the applied shear rate [33]. Until a specific threshold, which is known as yield stress, HIPEs respond like elastic solid. When the stress exceeded the threshold, HIPEs displayed a shear-thinning viscosity, i.e., non-Newtonian behaviour, for which the shear viscosity decreases with increasing

deformation rate [88], but their rheological profile varied appreciably as the internal phase amount and droplet size were changed. While non-Newtonian HIPEs show a limiting viscosity at low shear rates, an increase at shear rate has resulted in a spatial rearrangement of the molecules to follow the applied flow field and the structure of the system may change due to the breaking of weak bonds [33]. At slightly higher shear rates the flow curves show a linear behaviour, of which are caused by shear thinning.

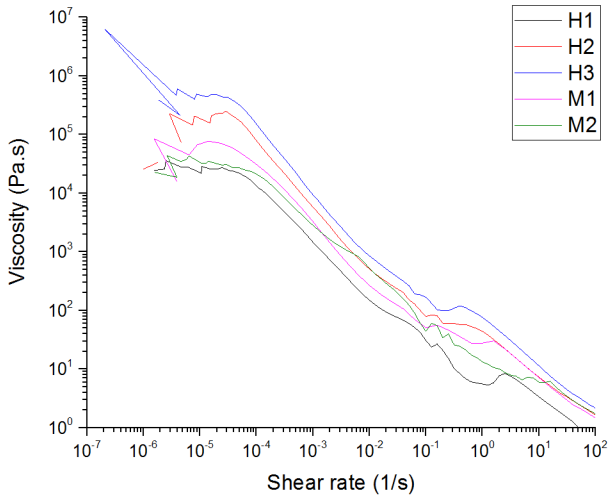

Figure 10: Shear-dependent viscosity data for M/HIPEs.

As the agitation rate of HIPEs during preparation increased from 600 rpm to 2000 rpm for H1-H3 samples (Table 1), the shear viscosity of the samples became greater (Figure 10). The increases in the viscosity of the HIPEs is related to the decreasing of the droplet size of the emulsion [89]. Due to the same reason, M1 prepared at 2000 rpm agitation rate has higher viscosity than M2 prepared at 1000 rpm agitation rate. Moreover, the higher internal phase amount also leds higher viscosity for water in oil emulsions [21]. Therefore, H2 and H3 have higher viscosity than MIPEs. On the other hand, due to the largest droplet size of H1, it has the lowest viscosity (Figure 10).

In order to compare test results with other rheological data, any intermediate shear stress / viscosity values can be calculated via best-fit equations. The viscosity curve in a given shear rate range for shear thinning systems can be fitted to the Carreau-Yasuda equation with the help of TRIOS data analysis [90] (Eq, 3)(Figure 11). The flow behaviour fitted to the Carreau-Yasuda model [91]:

$$\eta - \eta_\infty = \frac{(\eta_0 - \eta_\infty)}{\left[(1 + (\gamma/\gamma_c)^p)\right]^s} \quad \text{(Eq. 3)}$$

where η is the apparent viscosity (Pa s), η_∞ is the Newtonian limit viscosity at infinite shear rate (Pa s), η_0 is the zero-shear rate viscosity (Pa s), γ_c the critical shear rate for the end of the plateau at low shear rates (s^{-1}) and p and s are dimensionless constants which can be related to the exponent of the power law (n) by the operation ($1-p\times s$) [89].

Figure 11 shows the shear dependent viscosity data for H3 emulsion, after the data were fitted to Carreau-Yasuda equation, which were illustrated by the continuous blue line (other fitted lines are on the Appendix III). After the critical shear rates (γ_c) of M/HIPEs, which are approximately $3x10^{-5}$ s^{-1}, the emulsions were exposed of shear thinning behaviour related with increasing shear rate, which caused to decrease in viscosities of the emulsions (Table 4). Since the fluidity mainly depends on the viscosity of the liquid, shear thinning enables easier processing. Therefore, the resistance against the flow of the emulsions decreased due to the increase of the shear rate during printing.

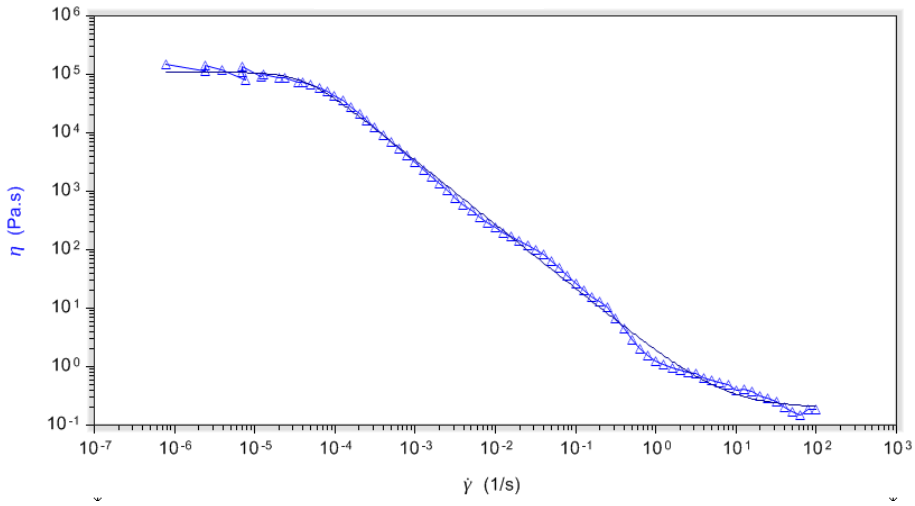

Figure 11: Shear-dependent viscosity data for H3 (Δ). Continuous lines illustrate data fitting to the Carreau–Yasuda model. Temperature = 25 °C.

Table 4: The fitting parameters of the Carreau-Yasuda equation for flow curves at 25 ºC.

	η_0 (Pa s)	η_∞ (Pa s)	γ_c (s^{-1})
H1	54434 ± 15285	2.6 ± 0.1	$3 \times 10^{-5} \pm 7 \times 10^{-6}$
H2	174911 ± 44021	2.9 ± 0.2	$2 \times 10^{-5} \pm 7 \times 10^{-6}$
H3	227299 ± 19381	1.6 ± 0.2	$3 \times 10^{-5} \pm 2 \times 10^{-6}$
M1	66473 ± 5864	3.5 ± 0.6	$2 \times 10^{-5} \pm 2 \times 10^{-6}$
M2	49765 ± 13860	3.3 ± 0.5	$6 \times 10^{-5} \pm 2 \times 10^{-6}$

4.2.2. Screen printing

Due to the suitability of the screen printing in many different areas, including additive layer deposition and patterning method in thick film technology [62], the colour filter for the liquid crystal display panel [64] and templating of micro-emulsion co-polymer onto cotton fabric [92], it can be applicable to produce macroporous polymer film. Moreover, besides low cost and productivity of the screen printing, the physical properties of the film, i.e., thickness, surface quality, pattern, can be tailored [60][64]. Therefore, this technique was tried to print macroporous polymer film from PUDA and EHA based M/HIPEs with different parameters during the printing in order to achieve open-porous film with thickness and good surface quality.

Screen-printings were performed using screen printer machine in Eurecat-CETEMMSA, Mataro, Spain. After the emulsion had been placed on the screen, it was spread using the steel blade from the opposite side of the squeegee. Then, the squeegee went over the screen with arranged pressure and angle to penetrate the emulsion on the substrate. The printed film was polymerized for 2 min in a water bath, which was needed to prevent the evaporation of the monomers from the emulsions to produce macroporous film. The presence of defects, one criterion for the quality of the films, was investigated by optical microscope (Industrial Microscope ECLIPSE LV1000, Nikon, Izasa S.A, Spain) (Figure 12). The light coloured area and the black dots indicated the roughness of the polyH(M)IPE films within a scale of 500 µm. The shining dots, which were due to the transmission of the light through the films, displayed the defects in the films.

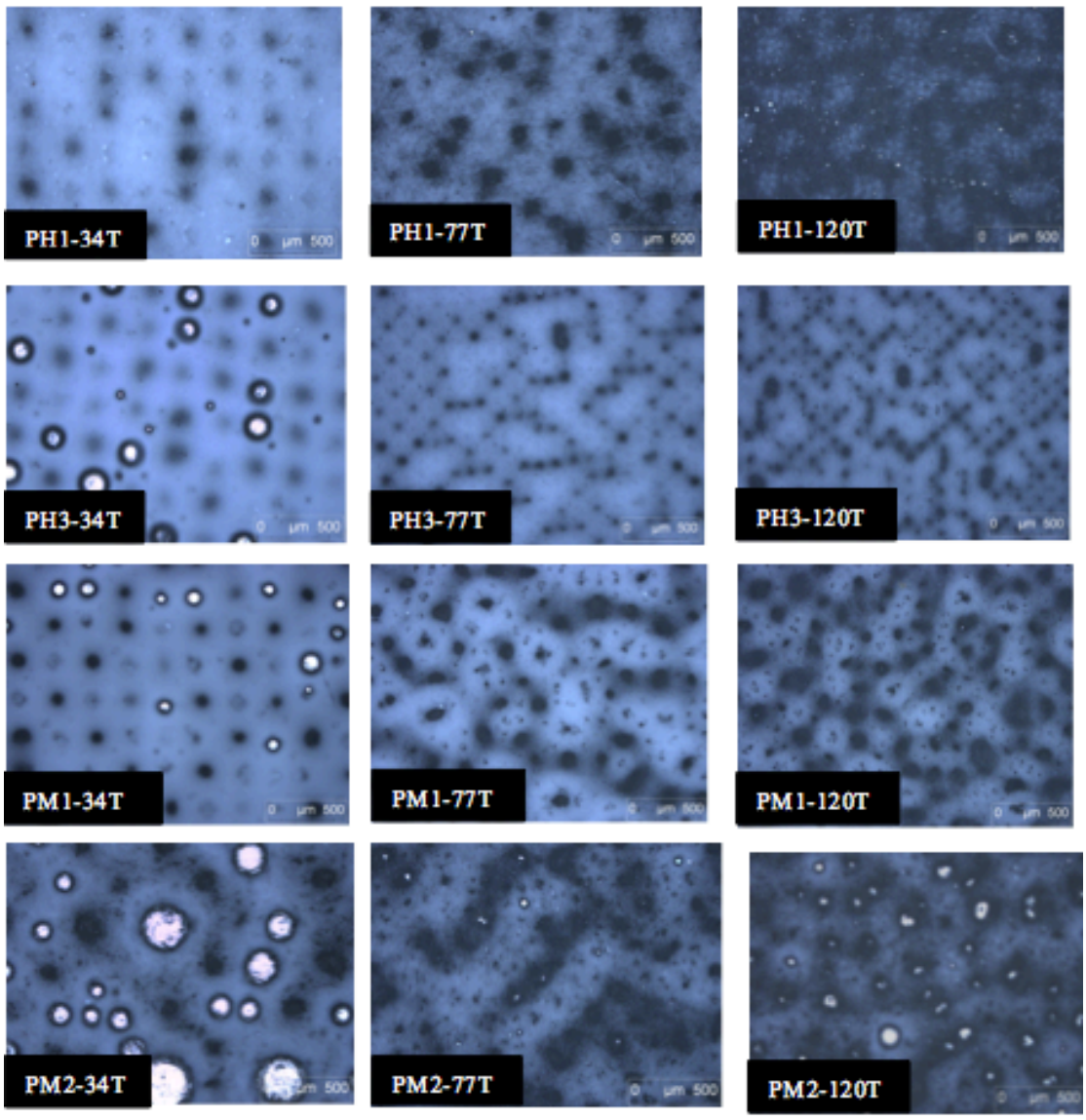

Figure 12: Surface properties of printed macroporous polymer films via optical microscope.

During the printing of H1 emulsion with 34T screen, of which have 34 threads per centimetre, the dark colour areas were observed on the corresponding fields under the cross sections of mesh wires and those areas increase with the increase of the threads per centimetre, which indicates the mesh size (Figure 12). The areas between the threads determine how much ink pass through the screen. Therefore, an increase in the threads per centimetre for the different screens having same mesh wire diameters causes the decrease of the open areas. Therefore, 77T and 120T screens have smaller open areas than 34T screen and that caused to pass less emulsion through the screen. On the other hand, H3 with the smallest droplet size has pinholes, when it was printed with 34T screen (Table 2)(Figure 12). During the printing, air bubbles might be captured inside of the emulsion because of the highest viscosity of H3 emulsion

(Figure 10) and they could not break due to the high open areas of the screen. However, when the printings were performed with 77T and 120T, the air bubbles were disrupted by printing through a screen with high mesh size. Moreover, due to the highest viscosity of H3 (Figure 10), the emulsion did not spread in the time frame between printing and polymerization. Therefore, it has more rough surface film than the other films printed with H1 (Figure 12).

PM1 printed with 34T screen had pinholes, which were in equipoised under the cross section of the threads. The reason of that was captured air bubbles in the emulsion same as PH3 film. However, due to the lower viscosity of M1 than H3, pinhole amount and size were smaller than that on the PH3 film. When the printings were performed with larger mesh size screens, i.e., 77T and 120T, the pinholes vanished because of increasing thread number per centimetre, but still the film did not have smooth surface. On the other hand, the printed films with M2 emulsion have different surface images than other films. The pinholes and dark areas show randomly distribution and have different sizes. This indicated that the pinholes were not a result of air capturing under the wire cross sections. After the blade had spread the emulsion onto the screen, evaporation of the monomers in the emulsions was promoted as the enlarged surface area of the emulsion film, therefore, the viscosity of the emulsion increased simultaneously. In case of M2 where SBS was dissolved in the continuous phase: the loss of the monomers (solvent) can lead to a significant increase in the viscosity of the emulsion. The subsequent transfer of the emulsion films from the screen to the substrate was therefore not as effective as for other emulsions. This led to the resulting polyMIPE film with the more defects compared to other screen printed polyH(M)IPE films.

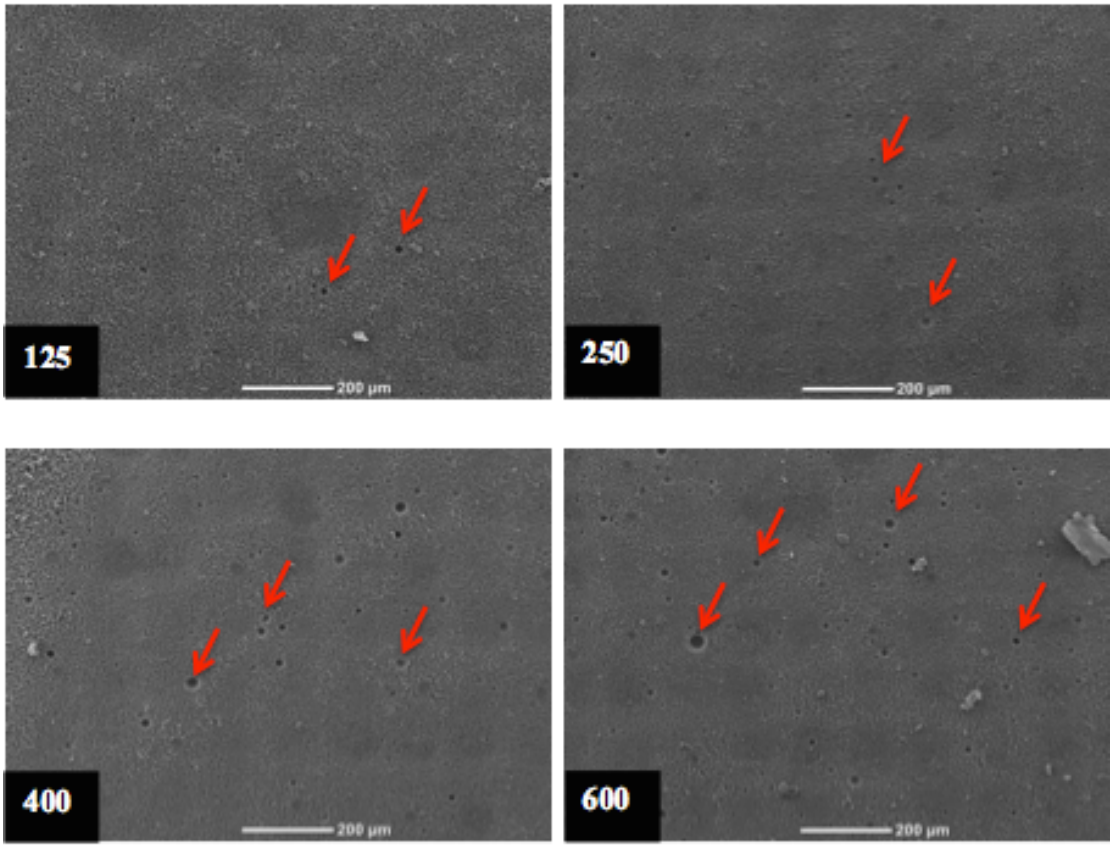

Figure 13: The SEM micrograph of the surface of H3 printed with 77T screen at different speeds.

In order to investigate the effect of squeegee speed on the pinhole amount, the emulsions were printed using 77T screen with different speeds, which were 125 mm/s, 250 mm/s, 400 mm/s and 600 mm/s. 77T screen was chosen for squeegee speed research, because the captured air in the highly viscos emulsion cannot be sheared during the printing with the low mesh size screen and that caused more pinholes in the film, which makes it difficult to investigate the printing speed (Figure 12). The increase in the pinhole number (red arrows in Figure 13) was observed from the SEM images with the rising of the printing speed. Fast printing causes air bubbles to form in the film through that transfer into the mesh openings. Despite the quality of the films, all polyH(M)IPE films processed open-porous surface, making the films applicable in terms of good permeability, e.g. as the separator for batteries (Figure 14).

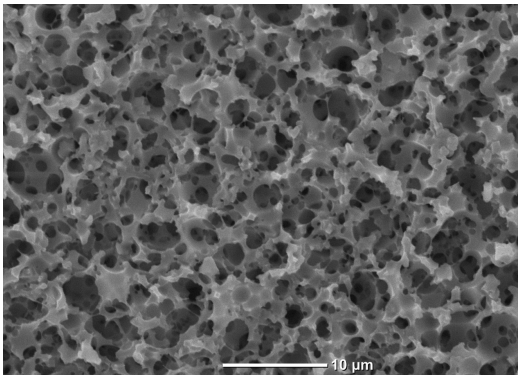

Figure 14: The SEM micrograph of the surface of PH3 printed with 62T screen.

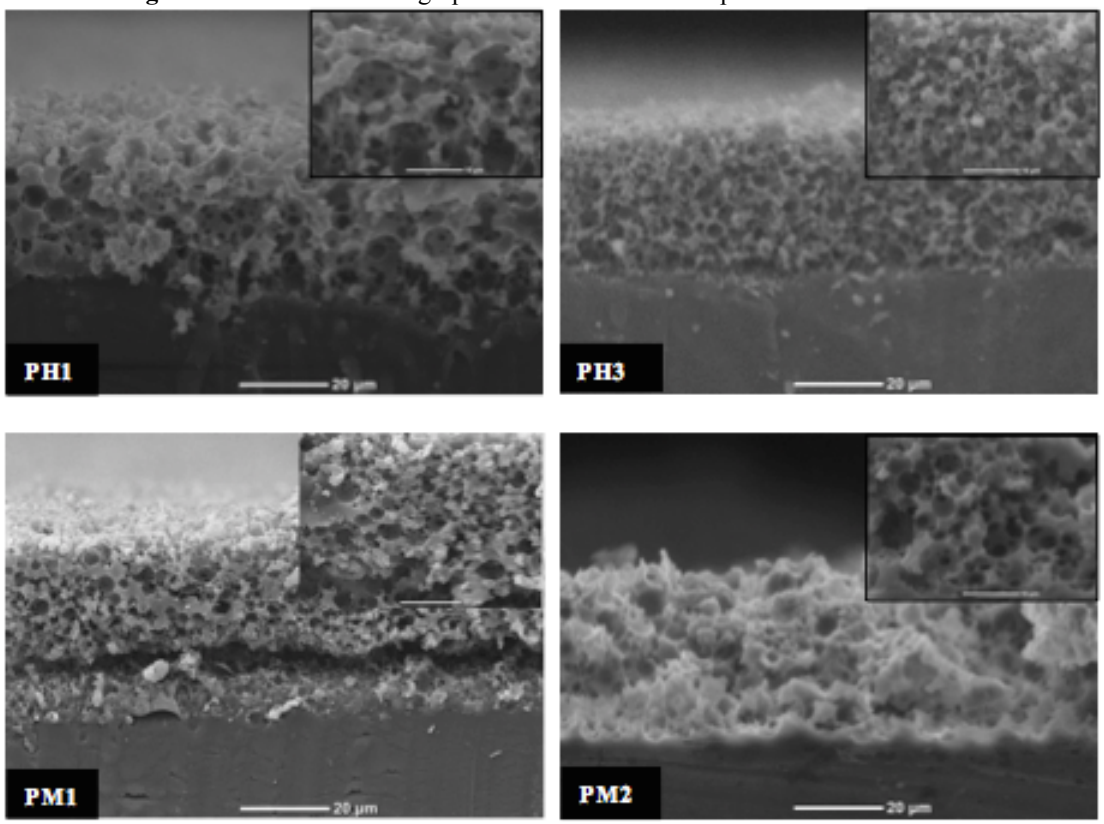

Figure 15: The SEM micrograph of the cross section of the printed polyH(M)IPE with 62T screen.

The Figure 15 shows the cross section of the screen printed macroporous polymer films and the high magnification SEM images show the open-porous and interconnected structures of the films, which was as expected as they were produced using surfactant-stabilized-emulsions (Table 1). The pore sizes were identical within error to the monoliths indicating that the screen-printing did not damage the structure of the emulsions. Furthermore, the cross sections of the films indicated to the good spreading of the emulsion. While PH1, PH3 and PM1 samples have well dispersed layers, unevenly spreading of PM2, polyMIPE with SBS, macroporous film can be observed both the surface images of the film (Figure 12) and the cross section (Figure 15 and Appendix IV). Therefore, the thicknesses of PM2 were not investigated.

Table 5: Thickness properties of screen-printed macroporous polymer samples (all results are μm).

Samples	Mesh size of the screen						
	34T	**62T (3 mm)[1]**	**62T (5 mm)[1]**	**62T (7 mm)[1]**	**77T**	**120T**	**A-200**
PH1	40 ± 5	30 ± 2	29 ± 2	31 ± 2	19 ± 5	x[1]	22 ± 3
PH3	35 ± 17	24 ± 2	27 ± 5	23 ± 3	x[2]	x[2]	x[2]
PM1	32 ± 4	30 ± 3[3]	26 ± 3	26 ± 3	x[2]	14 ± 2	x[2]

[1] the height of the screen from the substrate.
[2] x signs could not be calculated due to damage that occurred during the cutting of thin-film.
[3] The thickness of the film might not accurate due to the separation between film and substrate.

The screen mesh count, which is the number of wires per linear inch, is a critical factor for controlling printing thickness [61]. As a result of increasing thread number per centimetre, the open areas of the screens having the same thread diameter decreased. Therefore, the amount of emulsion could be deposited on to the same substrate are dropped during printing with the identical squeegee angle and pressure and resulted a decrease on the film thickness. The thickest macroporous polymer film was achieved by printing with 34T screen due to the largest open areas. However the thickness of films printed with 77T, A-200 and 120T cannot be calculated due to damage that occurred during the cutting of the thin films (Table 5). Although the thickest sample was achieved with 34T screen, it has not the smoothest surface as it contained many pinholes and was rough as seen in the optical microscope images (Figure 12). Furthermore, while the thickness of PH1 and PH3 film decrease sharply between printed with 34T and 62T screens from 40 μm to 30 μm and from 35 μm to 24 μm, respectively, the thickness of PM1 film did not change significantly (Table 5). This is surprising as H1 and H3 possess similar porosities; only the droplet size of H3 is smaller. This indicates that there are additional factors than viscosity and droplet size of the emulsion, which contribute to the thickness of the printed films. According to Kapur et. all. [93], not only shear rheology but also elasticity and yield stress important parameters and the interaction of the squeegee with the mesh plays also an important role on determining printing thickness. Moreover, an increase in the distance of the screen and the substrate during the printing with 62T screen did not affect the film thicknesses dramatically for all printed films, while other printing were performed with 3 mm height of the screen from the substrate. The thicknesses of the PH1 macroporous film printed with 77T and A-200 can be calculated and their

thicknesses were identical within error (Table 5). Those screens have similar mesh sizes but different screen materials. Therefore, the material of the screen was not affected on the thickness of polyHIPE.

The surface properties and thickness can be arranged both by changing printing conditions, e.g., mesh size, printing speed and viscosity of the emulsion during creating macroporous polymer film from acrylate based M/HIPE. Screen printing is a suitable technique if thin macroporous polymer films are required. However, a spring element should reach higher thickness than the films produced by the screen printing. Therefore, syringe printing technique has been investigated.

4.2.3. Syringe Printing

Syringe printing is a flexible method for creating 2D and 3D patterns; therefore, it was applicable to produce the required micropatterned cage-spring element. Therefore, a cage pattern was programmed in CAT as shown in Figure 16. This pattern was printed using emulsions H3 and M2, that were selected as inks because H3 has a high zero shear rate viscosity (Figure 10) and because the resulting polyMIPE PM2 a possessed lower viscoelastic deformation compared to PM1 (Figure 9).

$$\alpha = s \cdot \pi \cdot \left(\frac{d}{2}\right)^2 \qquad \text{(Eq. 4)}$$

The distance between the tip of the needle and the polyethylene terephthalate (PET) film used as substrate was set to be equal to the outer diameter (OD) of the needle. If the distance was smaller than the OD of the needle, the tip of the needle sank into the emulsion. On the other hand, if the distance was larger than the OD of the needle, the printed emulsion spread on the substrate. The dispersion rate (α) was calculated based on the OD of the needle (0.7 mm or 0.5 mm) and printing speed (5 mm/s) (Eq. 4). During the syringe printing, the needle moved to create a single cage continuously instead of moving in one long line and passing through on it to create cages, in order to prevent overlapping in the corners of the cages (Figure 16). Consequently, the needle did not pass through on the same point twice. Nevertheless, it moved close to the other point on the corner in order to create the desired shape. This caused the printed ink to overlap at the corners of the cages as indicated by the red circles during the printing process with dispersion rate α. Hence, the height of the walls of the cages

was lower than the height of the corner of the cages because the emulsion ink wetted the substrate. To reduce the undesired overlap, the dispersion rate was reduced by multiplying a factor of 0.75.

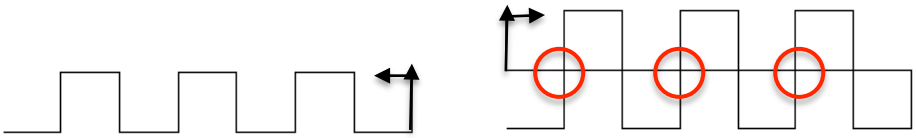

Figure 16: The first line of the pattern of 3D printing (left) and the following line (right).

Moreover, the dimension of the cage can be easily changed by changing the coordinates of the programmed patterns (Appendix V). After printing the cage pattern, the printed emulsion was polymerized and dried using the same conditions as described in section 4.2.2. The surface of the printed polyH(M)IPE cages were found to have an open-porous surface, which guaranties the permeability to allow for gas flow in the device during use (Figure 17).

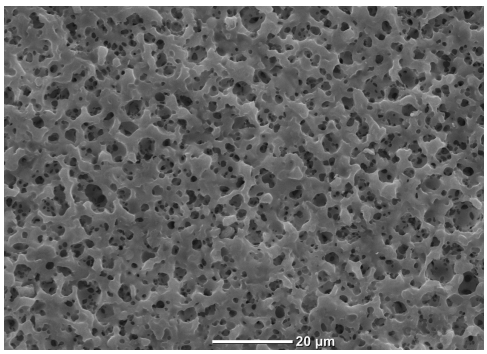

Figure 17: The SEM micrograph of the surface of PH3 printed with 0.7 mm outer diameter needle.

The cross-section of the walls had a prolate semi-ellipsoid shape. The reason of this was the wetting behaviour of the inks on the substrate. Nevertheless, the printed M/HIPE lines did not spread completely into thin films, but retained some height at the 2 min time frame between the printing and the polymerization (Figure 18). While the bottom width of the walls represent the spreading of the emulsion before polymerisation, the width at the middle height of the walls are important due to the forming of expansion of the spring element during the compression mainly there. Moreover, in order to determine the effect of the outer diameter of the needle on the height of the walls, those three dimensions of the printed macroporous polymer were calculated and compared each other.

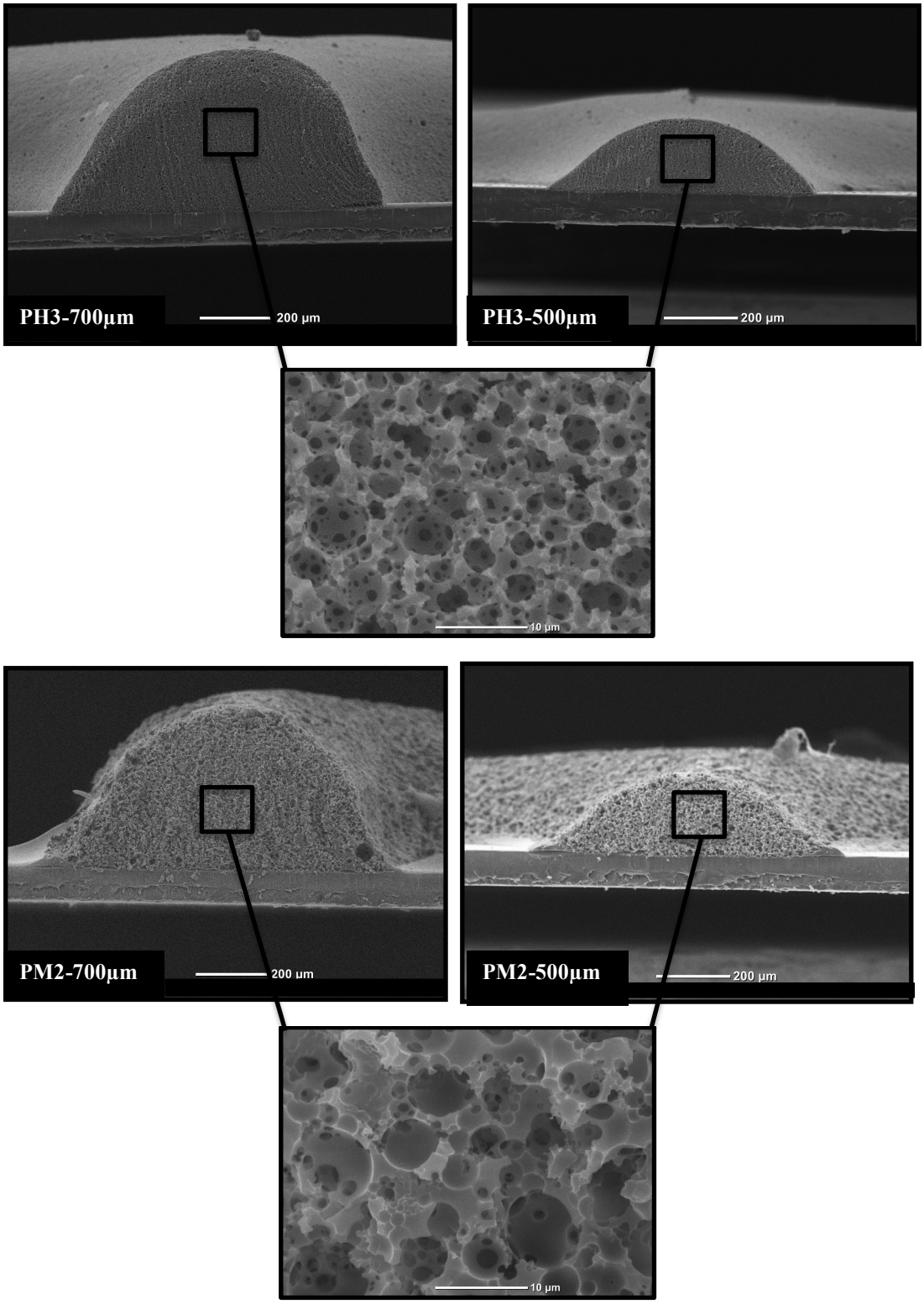

Figure 18: SEM images of PH3 and PM2 macroporous cages printed with 0.7 mm OD needle and 0.5 OD needle with α-75% dispense rate (The porous structure of polyH(M)IPE was shown on the right corners of printed with 0.5 mm OD needle).

The wall height and the bottom width of PH3 and PM2 printed with a 700 µm OD needle had 450 µm and 900 µm, respectively (Table 6). The half width of the walls were less than the bottom widths, which indicated the limited spreading of the

emulsions, due to the wetting of the inks on the substrates, prior to being polymerised. However, the fast UV polymerisation of the HIPE and MIPE only left a 2 min window for the emulsions to spread. Within this time frame the high zero-shear rate viscosity of the emulsions hindered effectively the spreading the inks (Table 4). Therefore, after the polymerisation, the resulting polyHIPE and polyMIPE walls remained 64% of the expected height of the walls. Furthermore, both polyH(M)IPE walls also possessed open-porous structures (Figure 18) with pore sizes of 3 ± 1 μm (PH3) and 5 ± 2 μm (PM2), and pore throat sizes of 0.6 ± 0.2 (PH3) and 1.5 ± 0.5 (PM2) respectively, identical within error to the monolithic polyH(M)IPEs indicating that the emulsion structures were unaffected by the printing process through a needle.

Table 6: Dimensions of PH3 and PM2 printed with α-75 % dispense rate measured from SEM images (All results are μm).

	700 μm OD Needle			**500 μm OD Needle**		
	Height	***Width***	***Bottom Width***	***Height***	***Width***	***Bottom Width***
PH3	430 ± 26	632 ± 10	889 ± 23	208 ± 8	503 ± 16	747 ± 29
PM2	475 ± 9	656 ± 26	872 ± 60	212 ± 9	415 ± 23	700 ± 15

PH3 and PM2 resulted from the polymerisation of the H3 and M2 printed with 500 μm OD needle had walls height of 210 μm and bottom width of 720 μm, respectively. Bottom width of the walls decreased to 23% due to the decrease in the OD of the needle to 29%, while the height of the walls decreased to 53%, respectively (Table 6). The drop in the bottom width affected on a decrease in the OD of the needle with same ratio, because bottom width is related with the wettability between the emulsion and the substrate. However, the heights of the walls depend on both the wettability and the dispersion rate of the emulsion, which is proportional to the square of the OD of the needle. Therefore, the dispersion rate of the emulsion dropped sharply and resulted much lower height of the walls than printed with 0.7 mm OD needle.

Cage shape pattern with desired thickness suitable for REWOD energy harvester could be produced by syringe printing. Therefore, the mechanical loading of the printed micropatterned spring on PET films were simulated by dynamic mechanical tests simulating a human walking. Moreover, the functionality of polyH(M)IPE cages as spring/spacer element was demonstrated by building a simple prototyped REWOD device.

4.2.4. Cyclic compression test results of syringe printed macroporous polymers

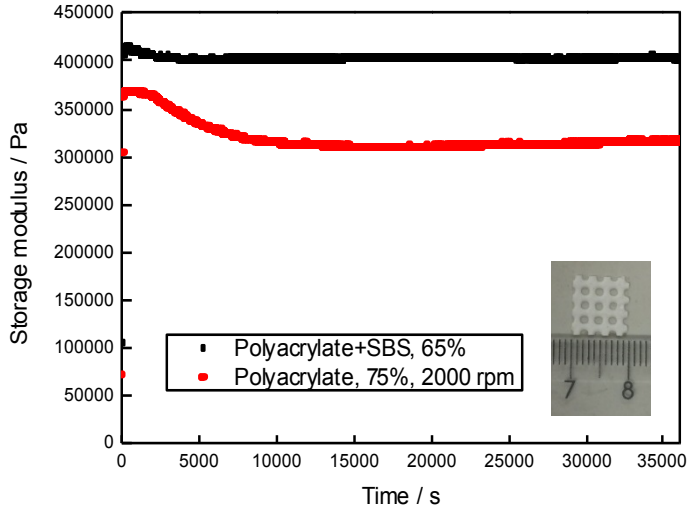

Figure 19: Storage modulus of syringe printed PH3 (red curve) and PM2 (black curve) cages from dynamic mechanical tests at a frequency of 2 Hz.

Although the cyclic compression tests on the polyH(M)IPE monoliths were conducted; it is impossible to run the cyclic test at 2 Hz, which is the step frequency of human walking, on the Universal mechanical testing machine. Therefore, in order to investigate the long-term mechanical behaviour of the samples under at realistic conditions, dynamic compression tests were performed on the printed micropatterned spring on PET films (10 mm x 10 mm, Figure 19) at 2 Hz and compressed by 30% of their original heights at 10 h. The storage modulus of the PH3 and PM2 patterned springs decreased over a period of time to remain eventually constant (Figure 19). When the storage modulus of polyHIPE was constant, it had decrease by 16% after 10000 s, the modulus of polyMIPE (3% decrease) remained constant within 2000 s after the measurement started. A residual strain occurred on the compressed samples beyond their elastic deformation region and also until equilibrium was reached, the residual strain accumulated after each cycle due to the Mullins softening effect [84]. As known from the results of the cyclic compression tests of the monoliths (Figure 8 and 9), PM2 had lower residual strain than PH3. Therefore, the low rate of the decrease in storage modulus of PM2 can be related to the lower residual strain. Furthermore, the constant moduli of the two samples after the initial reduction does

demonstrate their constant mechanical behaviour, indicating that both polyH(M)IPE cages were suitable for long term applications at the desired frequency.

4.2.5. Energy harvesting test of syringe printed macroporous polymers

The effectiveness of polyH(M)IPE cages as spring/spacer element was evaluated via a simple prototyped REWOD device. H3 and M2 emulsions were printed on the Mylar® Dielectric polyester layer laminated on to a cupper. After 16 Hg droplets of 450 µm in diameter were carefully placed in 16 cages, the pattern was closed with another cupper plate and connected to the voltammeter to measure the capacitance change of the device during the deformation and recovery of the Hg droplets, which wet the dielectric during compression and dewet during unloading (Figure 20).

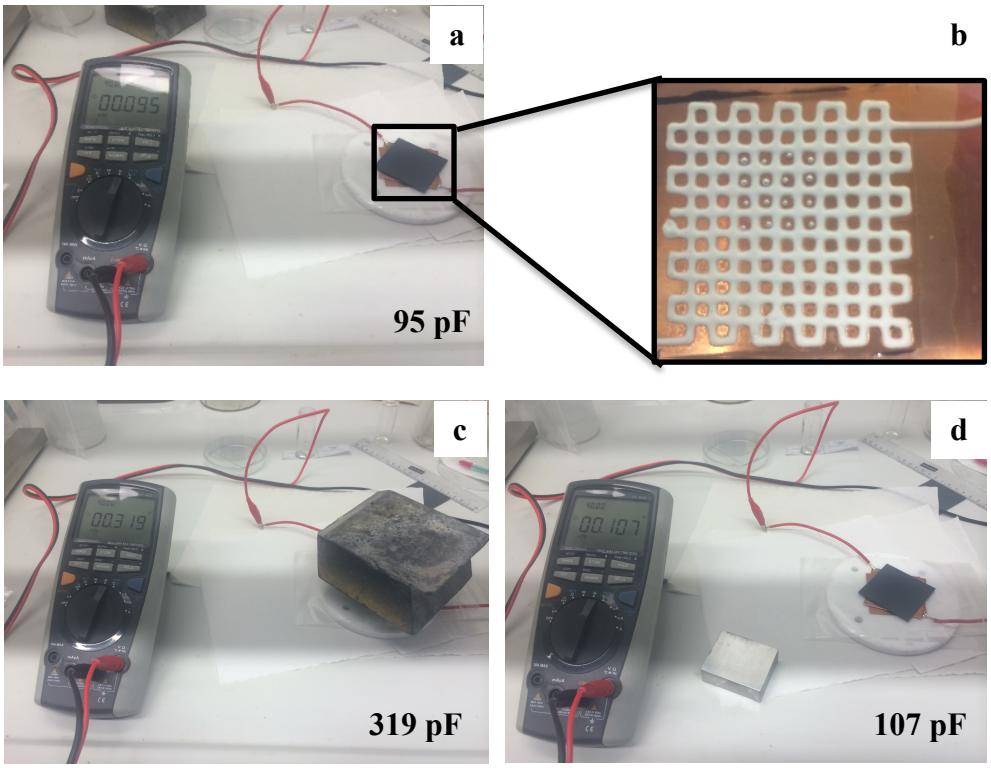

Figure 20: Photographs of the model REWOD energy harvester; the capacitance change of energy harvester prototype (photo a) incorporating with polyMIPE patterned spring elements containing Hg droplets (photo b). After the weight was added on the prototype (Photo c), and after the weight was removed from the prototype (photo d).

In order to achieve deformation and recovery of Hg droplets, a weight, which resulted in a cyclically applied compression load of 0.1 MPa, which is an estimated maximum compression load of an average weight person on the device, was placed on (Figure 20c) and removed from the REWOD device (Figure 20d). The device with polyMIPE cages was performed. The capacitance was measured as about 95 pF under zero external force. The reason of the low capacitance is small wetting area between the

Hg droplets and the dielectric (Figure 1a). The capacitance increased to 319 pF with applying a compression load of 0.1 MPa as a result of the increased wetted area of Hg on the dielectric caused by the deformation of the droplets. This indicates that the Hg droplets deformed under the load due to the compression of polyMIPE. After the removal of the compression load, the capacitance decreased to 107 pF. Even though the capacitance dropped due to the decreasing the wetted area of Hg on the dielectric, it did not recover fully to the original value. This can be explained by the residual strain of the polyMIPE cage due to viscoelastic deformation, which was also observed during cyclic compression tests of the monolithic control samples. This stopped the Hg droplets recovering to the original height.

At the other measurement of capacitance change, the device with polyHIPE cages under zero external force exhibited a capacitance of about 100 pF. After the weight was placed on the device, the capacitance increased to 670 pF. The reason of the higher capacitance value at the identical pressure was the lower elastic modulus of the polyHIPE. Due to the less compressed polyMIPE, Hg droplets deformed fewer and thus produced a smaller contact area with the dielectric than the device with polyHIPE cages. After the weight was removed, the capacitance decreased to 150 pF. This was, again, caused by the residual strain of the polyHIPE, which stopped the Hg droplets recovering to the original height. Moreover, due to the higher viscoelastic deformation of PH3 than PM2 (Figure 9), the difference of the starting and final capacitance of polyMIPE was about 11%, while it was 50% for polyHIPE.

5. Conclusions

The main objective of this work was to produce a spring/spacer element for use in a REWOD energy harvesting system. To realise practical REWOD harvesters, a patterned spring element is required to aid the reversible dewetting of liquid metal drops, which furthermore have to be kept separated. Therefore, flexible and durable macroporous polymers were synthesized and processed into micropatterned spring/spacer element to realise this element for REWOD device.

Firstly, emulsion templates using PUDA and EHA as monomers in the continuous phase were formulated and UV polymerized to produce macroporous poly(PUDA-co-EHA). The resulting macroporous polymers had an open porous structure. Their pore and pore throat diameters were directly related to the agitation rate during the emulsification and they were found to range form 8.4 μm to 2.8 μm for macroporous polymers prepared with the same internal phase volume but decreased with increasing agitation rate of the emulsion template. The macroporous polymers are flexible with elastic modulus in the range of 0.26 to 0.62 MPa. The less porous macroporous polymers had a higher modulus. The reversible and stabile compressibility of flexible polyH(M)IPEs were proven by the cyclic compression tests up to 70% of their original height. Additionally, long-term compressible and durable behaviour of the printed macroporous polymers was verified via DMA under the simulated conditions.

M/HIPEs were processed into spring elements by printing methods. Open porous-surfaces of thin films were produced via the screen printing. It was found that, the film quality was affected by the viscosity of the emulsions, the printing speed and the mesh size of the screen. On the other hand, although the screen printing method did not damage on the porous structure of macroporous polymer, the desired thickness of the spring element could not be achieved, but it can be viable option to produce thin macroporous polymer films. Afterwards, M/HIPEs were successfully printed with syringe printer in a desired cage pattern controlled via software program, which also helped to adjust the pattern, coordinates and the printing speed. By using the different outer diameters needles, the thicknesses of the walls could be controlled.

Finally, a REWOD prototype was designed and built by placing Hg droplets into the as-produced polyH(M)IPE spring cages to demonstrate the feasibility of a functional REWOD device. The working principal of the polyH(M)IPE spring cages was proven

producing a maximum capacitance change of 570 pF of the prototype REWOD device during application and removal of an external compression load, caused by the changing wetting area of Hg droplets on the dielectric. This proved that, polyH(M)IPEs were successfully processed into flexible and durable macroporous polymers springs by syringe printing that can be used in REWOD energy harvesting systems.

6. References

[1] T. Krupenkin and J. A. Taylor, “Reverse electrowetting as a new approach to high-power energy harvesting,” *Nat. Commun.*, vol. 2, p. 448, Aug. 2011.

[2] L. K. J, *Continuous process for the preparation of emulsions*. Google Patents, 1971.

[3] J. Xu and J. Tang, “Linear stiffness compensation using magnetic effect to improve electro-mechanical coupling for piezoelectric energy harvesting,” *Sens. Actuators Phys.*, vol. 235, pp. 80–94, Nov. 2015.

[4] K. Kleiner, “Nuclear energy: assessing the emissions,” *Nat. Rep. Clim. Change*, no. 0810, pp. 130–131, Oct. 2008.

[5] J. Goldemberg, United Nations Development Programme, United Nations, and World Energy Council, Eds., *World energy assessment: energy and the challenge of sustainability*. New York, NY: United Nations Development Programme, 2000.

[6] P. D. Mitcheson, E. M. Yeatman, G. K. Rao, A. S. Holmes, and T. C. Green, “Energy Harvesting From Human and Machine Motion for Wireless Electronic Devices,” \iProc. IEEE, vol. 96, no. 9, pp. 1457–1486, Sep. 2008.

[7] P. S. Liu, *Porous materials: processing and applications*, 1st edition. Waltham, MA: Elsevier, 2014.

[8] D. Wu, F. Xu, B. Sun, R. Fu, H. He, and K. Matyjaszewski, “Design and Preparation of Porous Polymers,” *Chem. Rev.*, vol. 112, no. 7, pp. 3959–4015, Jul. 2012.

[9] J. Rouquerol, D. Avnir, C. W. Fairbridge, D. H. Everett, J. M. Haynes, N. Pernicone, J. D. F. Ramsay, K. S. W. Sing, and K. K. Unger, “Recommendations for the characterization of porous solids (Technical Report),” *Pure Appl. Chem.*, vol. 66, no. 8, Jan. 1994.

[10] N. B. McKeown and P. M. Budd, “Exploitation of Intrinsic Microporosity in Polymer-Based Materials,” *Macromolecules*, vol. 43, no. 12, pp. 5163–5176, Jun. 2010.

[11] Q. Xu, Ed., *Nanoporous materials: synthesis and applications*. Boca Raton, Fla: CRC, 2013.

[12] S. A. Johnson, P. J. Ollivier, and T. E. Mallouk, "Ordered mesoporous polymers of tunable pore size from colloidal silica templates," *Science*, vol. 283, no. 5404, pp. 963–965, Feb. 1999.

[13] S. A. Al-Muhtaseb and J. A. Ritter, "Preparation and Properties of Resorcinol-Formaldehyde Organic and Carbon Gels," *Adv. Mater.*, vol. 15, no. 2, pp. 101–114, Jan. 2003.

[14] B. Tian, S. A. Shankarappa, H. H. Chang, R. Tong, and D. S. Kohane, "Biodegradable Mesostructured Polymer Membranes," *Nano Lett.*, vol. 13, no. 9, pp. 4410–4415, Sep. 2013.

[15] R. M. Capito, H. S. Azevedo, Y. S. Velichko, A. Mata, and S. I. Stupp, "Self-assembly of large and small molecules into hierarchically ordered sacs and membranes," *Science*, vol. 319, no. 5871, pp. 1812–1816, Mar. 2008.

[16] Y. Meng, D. Gu, F. Zhang, Y. Shi, H. Yang, Z. Li, C. Yu, B. Tu, and D. Zhao, "Ordered mesoporous polymers and homologous carbon frameworks: amphiphilic surfactant templating and direct transformation," *Angew. Chem. Int. Ed Engl.*, vol. 44, no. 43, pp. 7053–7059, Nov. 2005.

[17] Q. Jiang, A. Menner, and A. Bismarck, "Emulsion-templated macroporous polymer/polymer composites with switchable stiffness," *Pure Appl. Chem.*, vol. 86, no. 2, Jan. 2014.

[18] M. S. Silverstein, "Emulsion-templated porous polymers: A retrospective perspective," *Polymer*, vol. 55, no. 1, pp. 304–320, Jan. 2014.

[19] M. S. Silverstein, N. R. Cameron, and M. A. Hillmyer, Eds., *Porous polymers*. Hoboken, N.J: Wiley, 2011.

[20] A. Menner, K. Haibach, R. Powell, and A. Bismarck, "Tough reinforced open porous polymer foams via concentrated emulsion templating," *Polymer*, vol. 47, no. 22, pp. 7628–7635, Oct. 2006.

[21] M. Tebboth, A. Kogelbauer, and A. Bismarck, "Highly permeable macroporous polymers via controlled agitation of emulsion templates," *Chem. Eng. Sci.*, vol. 137, pp. 786–795, Dec. 2015.

[22] Kenneth J. Lissant, “Continuous Process for the prepartion of emulsion,” US 3565817.

[23] J. M. Williams and D. A. Wrobleski, “Spatial distribution of the phases in water-in-oil emulsions. Open and closed microcellular foams from cross-linked polystyrene,” *Langmuir*, vol. 4, no. 3, pp. 656–662, May 1988.

[24] R. Owen, C. Sherborne, T. Paterson, N. H. Green, G. C. Reilly, and F. Claeyssens, “Emulsion templated scaffolds with tunable mechanical properties for bone tissue engineering,” *J. Mech. Behav. Biomed. Mater.*, vol. 54, pp. 159–172, Feb. 2016.

[25] N. R. Cameron and D. C. Sherrington, “Preparation and glass transition temperatures of elastomeric PolyHIPE materials,” *J. Mater. Chem.*, vol. 7, no. 11, pp. 2209–2212, 1997.

[26] S. Jerenec, M. Šimić, A. Savnik, A. Podgornik, M. Kolar, M. Turnšek, and P. Krajnc, “Glycidyl methacrylate and ethylhexyl acrylate based polyHIPE monoliths: Morphological, mechanical and chromatographic properties,” *React. Funct. Polym.*, vol. 78, pp. 32–37, May 2014.

[27] A. Menner, R. Verdejo, M. Shaffer, and A. Bismarck, “Particle-Stabilized Surfactant-Free Medium Internal Phase Emulsions as Templates for Porous Nanocomposite Materials: poly-Pickering-Foams,” *Langmuir*, vol. 23, no. 5, pp. 2398–2403, Feb. 2007.

[28] A. Menner, R. Powell, and A. Bismarck, “Open Porous Polymer Foams via Inverse Emulsion Polymerization: Should the Definition of High Internal Phase (Ratio) Emulsions Be Extended?,” *Macromolecules*, vol. 39, no. 6, pp. 2034–2035, Mar. 2006.

[29] I. Pulko, V. Smrekar, A. Podgornik, and P. Krajnc, “Emulsion templated open porous membranes for protein purification,” *J. Chromatogr. A*, vol. 1218, no. 17, pp. 2396–2401, Apr. 2011.

[30] H. Zhang and A. I. Cooper, “Synthesis of Monodisperse Emulsion-Templated Polymer Beads by Oil-in-Water-in-Oil (O/W/O) Sedimentation Polymerization,” *Chem. Mater.*, vol. 14, no. 10, pp. 4017–4020, Oct. 2002.

[31] M. Sušec, S. C. Ligon, J. Stampfl, R. Liska, and P. Krajnc, “Hierarchically Porous Materials from Layer-by-Layer Photopolymerization of High Internal

Phase Emulsions," *Macromol. Rapid Commun.*, vol. 34, no. 11, pp. 938–943, Jun. 2013.

[32] E. Alzahrani, "Organic monolithic materials: preparation and applications," *Indian J. Appl. Res.*, vol. 5, no. 2, pp. 846–852, 2015.

[33] T. F. Tadros, *Rheology of dispersions: principles and applications*. Weinheim: Wiley-VCH-Verl, 2010.

[34] H. Kunieda, N. Yano, and C. Solans, "The stability of gel—emulsions in a water/nonionic surfactant/oil system," *Colloids Surf.*, vol. 36, no. 3, pp. 313–322, Jan. 1989.

[35] R. Wu, A. Menner, and A. Bismarck, "Macroporous polymers made from medium internal phase emulsion templates: Effect of emulsion formulation on the pore structure of polyMIPEs," *Polymer*, vol. 54, no. 21, pp. 5511–5517, Oct. 2013.

[36] V. O. Ikem, A. Menner, and A. Bismarck, "High-Porosity Macroporous Polymers Sythesized from Titania-Particle-Stabilized Medium and High Internal Phase Emulsions," *Langmuir*, vol. 26, no. 11, pp. 8836–8841, Jun. 2010.

[37] J. J. Blaker, K.-Y. Lee, X. Li, A. Menner, and A. Bismarck, "Renewable nanocomposite polymer foams synthesized from Pickering emulsion templates," *Green Chem.*, vol. 11, no. 9, p. 1321, 2009.

[38] L. L. C. Wong, V. O. Ikem, A. Menner, and A. Bismarck, "Macroporous Polymers with Hierarchical Pore Structure from Emulsion Templates Stabilised by Both Particles and Surfactants," *Macromol. Rapid Commun.*, vol. 32, no. 19, pp. 1563–1568, Oct. 2011.

[39] A. Barbetta and N. R. Cameron, "Morphology and Surface Area of Emulsion-Derived (PolyHIPE) Solid Foams Prepared with Oil-Phase Soluble Porogenic Solvents: Span 80 as Surfactant," *Macromolecules*, vol. 37, no. 9, pp. 3188–3201, May 2004.

[40] S. Livshin and M. S. Silverstein, "Cross-linker flexibility in porous crystalline polymers synthesized from long side-chain monomers through emulsion templating," *Soft Matter*, vol. 4, no. 8, p. 1630, 2008.

[41] S. D. Kimmins and N. R. Cameron, “Functional Porous Polymers by Emulsion Templating: Recent Advances,” *Adv. Funct. Mater.*, vol. 21, no. 2, pp. 211–225, Jan. 2011.

[42] M. Tebboth, A. Menner, A. Kogelbauer, and A. Bismarck, “Polymerised high internal phase emulsions for fluid separation applications,” *Curr. Opin. Chem. Eng.*, vol. 4, pp. 114–120, May 2014.

[43] P. Krajnc, N. Leber, D. Stefanec, S. Kontrec, and A. Podgornik, “Preparation and characterisation of poly(high internal phase emulsion) methacrylate monoliths and their application as separation media,” *J. Chromatogr. A*, vol. 1065, no. 1, pp. 69–73, Feb. 2005.

[44] C. Martin, J. Coyne, and G. Carta, “Properties and performance of novel high-resolution/high-permeability ion-exchange media for protein chromatography,” *J. Chromatogr. A*, vol. 1069, no. 1, pp. 43–52, Mar. 2005.

[45] V. O. Ikem, A. Menner, A. Bismarck, and L. R. Norman, “Liquid Screen: A Novel Method To Produce an In-Situ Gravel Pack,” *SPE J.*, vol. 19, no. 03, pp. 437–442, Jun. 2014.

[46] M. P, S. C, D. D, and T. P, “Functionalization of poly(high internal phase emulsion) with amine for co2 capture,” *Chem. Eng. Trans.*, pp. 391–396, Sep. 2013.

[47] O. Kulygin and M. S. Silverstein, “Porous poly(2-hydroxyethyl methacrylate) hydrogels synthesized within high internal phase emulsions,” *Soft Matter*, vol. 3, no. 12, p. 1525, 2007.

[48] Y. Lumelsky, J. Zoldan, S. Levenberg, and M. S. Silverstein, “Porous Polycaprolactone−Polystyrene Semi-interpenetrating Polymer Networks Synthesized within High Internal Phase Emulsions,” *Macromolecules*, vol. 41, no. 4, pp. 1469–1474, Feb. 2008.

[49] V. Shkolnikov, D. G. Strickland, D. P. Fenning, and J. G. Santiago, “Design and fabrication of porous polymer wick structures,” *Sens. Actuators B Chem.*, vol. 150, no. 2, pp. 556–563, Oct. 2010.

[50] D. W. Johnson, C. Sherborne, M. P. Didsbury, C. Pateman, N. R. Cameron, and F. Claeyssens, “Macrostructuring of Emulsion-templated Porous Polymers by 3D Laser Patterning,” *Adv. Mater.*, vol. 25, no. 23, pp. 3178–3181, Jun. 2013.

[51] M. Kittila, J. Hagberg, E. Jakku, and S. Leppavuori, “Direct Gravure Printing (DGP) Method for Printing Fine-Line Electrical Circuits on Ceramics,” *IEEE Trans. Electron. Packag. Manuf.*, vol. 27, no. 2, pp. 109–114, Apr. 2004.

[52] Z. Bao, J. A. Rogers, and H. E. Katz, “Printable organic and polymeric semiconducting materials and devices,” *J. Mater. Chem.*, vol. 9, no. 9, pp. 1895–1904, 1999.

[53] Z. Bao, A. Dodabalapur, V. R. Raju, and A. J. Lovinger, “High-Performance Plastic Transistors Fabricated by Printing Techniques,” *Chem. Mater.*, vol. 9, no. 6, pp. 1299–1301, Jun. 1997.

[54] D. A. Pardo, G. E. Jabbour, and N. Peyghambarian, “Application of Screen Printing in the Fabrication of Organic Light-Emitting Devices,” *Adv. Mater.*, vol. 12, no. 17, pp. 1249–1252, Sep. 2000.

[55] S. Ito, P. Chen, P. Comte, M. K. Nazeeruddin, P. Liska, P. Péchy, and M. Grätzel, “Fabrication of screen-printing pastes from TiO2 powders for dye-sensitised solar cells,” *Prog. Photovolt. Res. Appl.*, vol. 15, no. 7, pp. 603–612, Nov. 2007.

[56] F. C. Krebs, “Fabrication and processing of polymer solar cells: A review of printing and coating techniques,” *Sol. Energy Mater. Sol. Cells*, vol. 93, no. 4, pp. 394–412, Apr. 2009.

[57] A. Shafiee and A. Atala, “Printing Technologies for Medical Applications,” *Trends Mol. Med.*, vol. 22, no. 3, pp. 254–265, Mar. 2016.

[58] D. J. Thomas and T. C. Claypole, “3-D Printing,” in *Printing on Polymers*, Elsevier, 2016, pp. 293–306.

[59] S. C. Cox, J. A. Thornby, G. J. Gibbons, M. A. Williams, and K. K. Mallick, “3D printing of porous hydroxyapatite scaffolds intended for use in bone tissue engineering applications,” *Mater. Sci. Eng. C*, vol. 47, pp. 237–247, Feb. 2015.

[60] D. Novaković, N. Kašiković, G. Vladić, and M. Pál, “Screen Printing,” in *Printing on Polymers*, Elsevier, 2016, pp. 247–261.

[61] J. Pan, G. L. Tonkay, and A. Quintero, “SCREEN PRINTING PROCESS DESIGN OF EXPERIMENTS FOR FINE LINE PRINTING OF THICK FILM CERAMIC SUBSTRATES,” *J. Electron. Manuf.*, vol. 09, no. 03, pp. 203–213, Sep. 1999.

[62] E. Horvath, G. Harsanyi, G. Henap, and A. Torok, “Mechanical modelling and life cycle optimisation of screen printing,” *J. Theor. Appl. Mech. Vol 50 No 4 2012*, 2012.

[63] H. Kipphan, Ed., *Handbook of print media: technologies and production methods*. Berlin ; New York: Springer, 2001.

[64] T.-M. Lee, Y.-J. Choi, S.-Y. Nam, C.-W. You, D.-Y. Na, H.-C. Choi, D.-Y. Shin, K.-Y. Kim, and K.-I. Jung, “Color filter patterned by screen printing,” *Thin Solid Films*, vol. 516, no. 21, pp. 7875–7880, Sep. 2008.

[65] F. C. Godoi, S. Prakash, and B. R. Bhandari, “3d printing technologies applied for food design: Status and prospects,” *J. Food Eng.*, vol. 179, pp. 44–54, Jun. 2016.

[66] P. J. Nuñez, A. Rivas, E. García-Plaza, E. Beamud, and A. Sanz-Lobera, “Dimensional and Surface Texture Characterization in Fused Deposition Modelling (FDM) with ABS plus,” *Procedia Eng.*, vol. 132, pp. 856–863, 2015.

[67] A. Goyanes, H. Chang, D. Sedough, G. B. Hatton, J. Wang, A. Buanz, S. Gaisford, and A. W. Basit, “Fabrication of controlled-release budesonide tablets via desktop (FDM) 3D printing,” *Int. J. Pharm.*, vol. 496, no. 2, pp. 414–420, Dec. 2015.

[68] A. Goyanes, A. B. M. Buanz, A. W. Basit, and S. Gaisford, “Fused-filament 3D printing (3DP) for fabrication of tablets,” *Int. J. Pharm.*, vol. 476, no. 1–2, pp. 88–92, Dec. 2014.

[69] F. Scalera, C. Esposito Corcione, F. Montagna, A. Sannino, and A. Maffezzoli, “Development and characterization of UV curable epoxy/hydroxyapatite suspensions for stereolithography applied to bone tissue engineering,” *Ceram. Int.*, vol. 40, no. 10, pp. 15455–15462, Dec. 2014.

[70] F. P. W. Melchels, J. Feijen, and D. W. Grijpma, “A review on stereolithography and its applications in biomedical engineering,” *Biomaterials*, vol. 31, no. 24, pp. 6121–6130, Aug. 2010.

[71] F. P. W. Melchels, K. Bertoldi, R. Gabbrielli, A. H. Velders, J. Feijen, and D. W. Grijpma, “Mathematically defined tissue engineering scaffold architectures prepared by stereolithography,” *Biomaterials*, vol. 31, no. 27, pp. 6909–6916, Sep. 2010.

[72] A. J. Lopes, I. H. Lee, E. MacDonald, R. Quintana, and R. Wicker, “Laser curing of silver-based conductive inks for in situ 3D structural electronics fabrication in stereolithography,” *J. Mater. Process. Technol.*, vol. 214, no. 9, pp. 1935–1945, Sep. 2014.

[73] O. Dufaud and S. Corbel, “Oxygen diffusion in ceramic suspensions for stereolithography,” *Chem. Eng. J.*, vol. 92, no. 1–3, pp. 55–62, Apr. 2003.

[74] A. Licciulli, C. E. Corcione, A. Greco, V. Amicarelli, and A. Maffezzoli, “Laser stereolithography of ZrO2 toughened Al2O3,” *J. Eur. Ceram. Soc.*, vol. 24, no. 15–16, pp. 3769–3777, Dec. 2004.

[75] L. Elomaa, A. Kokkari, T. Närhi, and J. V. Seppälä, “Porous 3D modeled scaffolds of bioactive glass and photocrosslinkable poly(ε-caprolactone) by stereolithography,” *Compos. Sci. Technol.*, vol. 74, pp. 99–106, Jan. 2013.

[76] J. P. Kruth, X. Wang, T. Laoui, and L. Froyen, “Lasers and materials in selective laser sintering,” *Assem. Autom.*, vol. 23, no. 4, pp. 357–371, Dec. 2003.

[77] L. L. C. Wong, P. M. Baiz Villafranca, A. Menner, and A. Bismarck, “Hierarchical Polymerized High Internal Phase Emulsions Synthesized from Surfactant-Stabilized Emulsion Templates,” *Langmuir*, vol. 29, no. 20, pp. 5952–5961, May 2013.

[78] M. . Ruiz, P. Lermanda, and R. Padilla, “Drop size distribution in a batch mixer under breakage conditions,” *Hydrometallurgy*, vol. 63, no. 1, pp. 65–74, Jan. 2002.

[79] A. Menner and A. Bismarck, “New Evidence for the Mechanism of the Pore Formation in Polymerising High Internal Phase Emulsions or Why polyHIPEs Have an Interconnected Pore Network Structure,” *Macromol. Symp.*, vol. 242, no. 1, pp. 19–24, Oct. 2006.

[80] S. Keyf, “The modification of bitumen with reactive ethylene terpolymer, styrene butadiene styrene and variable amounts of ethylene vinyl acetate,” *Res. Chem. Intermed.*, vol. 41, no. 3, pp. 1485–1497, Mar. 2015.

[81] R.-S. Shih, S.-W. Kuo, and F.-C. Chang, “Thermal and mechanical properties of microcellular thermoplastic SBS/PS/SBR blend: effect of crosslinking,” *Polymer*, vol. 52, no. 3, pp. 752–759, Feb. 2011.

[82] J. M. Donelan, R. Kram, and A. D. Kuo, “Mechanical work for step-to-step transitions is a major determinant of the metabolic cost of human walking,” *J. Exp. Biol.*, vol. 205, no. 23, pp. 3717–3727, Dec. 2002.

[83] J. Bergstrom, “Constitutive modeling of the large strain time-dependent behavior of elastomers,” *J. Mech. Phys. Solids*, vol. 46, no. 5, pp. 931–954, May 1998.

[84] L. Mullins and N. R. Tobin, “Stress softening in rubber vulcanizates. Part I. Use of a strain amplification factor to describe the elastic behavior of filler-reinforced vulcanized rubber,” *J. Appl. Polym. Sci.*, vol. 9, no. 9, pp. 2993–3009, Sep. 1965.

[85] J. Wu, B. Guo, C.-M. Chan, J. Li, and H.-S. Tang, “Synergistic toughening effect of SBS and HDPE on the fracture of the PS/HDPE/SBS blends,” *Polymer*, vol. 42, no. 21, pp. 8857–8865, Oct. 2001.

[86] H.-W. Lin, C.-P. Chang, W.-H. Hwu, and M.-D. Ger, “The rheological behaviors of screen-printing pastes,” *J. Mater. Process. Technol.*, vol. 197, no. 1–3, pp. 284–291, Feb. 2008.

[87] R. Aucklah, “Ink formulation and rheological characterisation of zirconia screen printing inks,” Loughborough University, Leicestershire, UK, 2011.

[88] C. F. Welch, G. D. Rose, D. Malotky, and S. T. Eckersley, “Rheology of High Internal Phase Emulsions,” *Langmuir*, vol. 22, no. 4, pp. 1544–1550, Feb. 2006.

[89] M. C. García, M. C. Alfaro, and J. Muñoz, “Influence of the ratio of amphiphilic copolymers used as emulsifiers on the microstructure, physical stability and rheology of α-pinene emulsions stabilized with gellan gum,” *Colloids Surf. B Biointerfaces*, vol. 135, pp. 465–471, Nov. 2015.

[90] G. A. SCHRAMM and G. H. (Firm), *A Practical Approach to Rheology and Rheometry*. Haake, 1994.

[91] K. Yasuda, R. C. Armstrong, and R. E. Cohen, “Shear flow properties of concentrated solutions of linear and star branched polystyrenes,” *Rheol. Acta*, vol. 20, no. 2, pp. 163–178, Mar. 1981.

[92] M. A. Abd El-Ghaffar, F. A. Kantouch, Z. M. Mahmoud, K. Haggag, A. I. Hashem, and A. A. Ramadan, “Micro-emulsion co-polymerisation of butyl acrylate with acrylic acid as binder for textile pigment printing,” *Pigment Resin Technol.*, vol. 43, no. 2, pp. 84–91, Feb. 2014.

[93] N. Kapur, S. J. Abbott, E. D. Dolden, and P. H. Gaskell, “Predicting the Behavior of Screen Printing,” *IEEE Trans. Compon. Packag. Manuf. Technol.*, vol. 3, no. 3, pp. 508–515, Mar. 2013.

Appendix

Appendix I Stress-strain curves of PH3 via cyclic test with 70% strain rates.

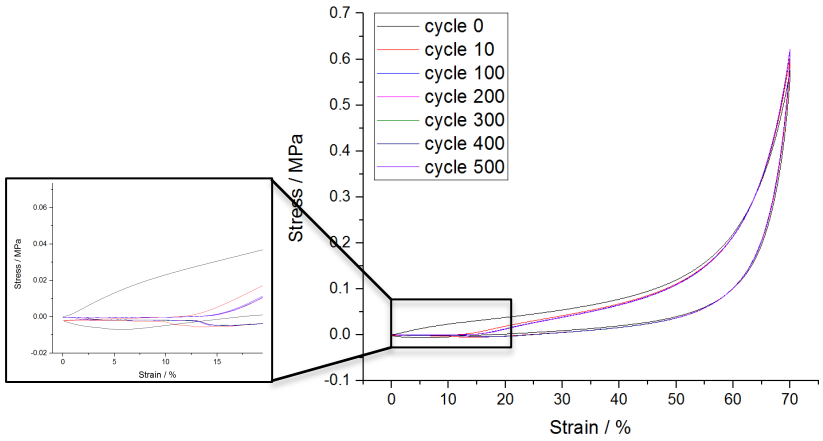

Appendix II Stress-strain curves of PM2 via cyclic test with 10% (a), 20% (b), 40% (c) and 70% (d) strain rates.

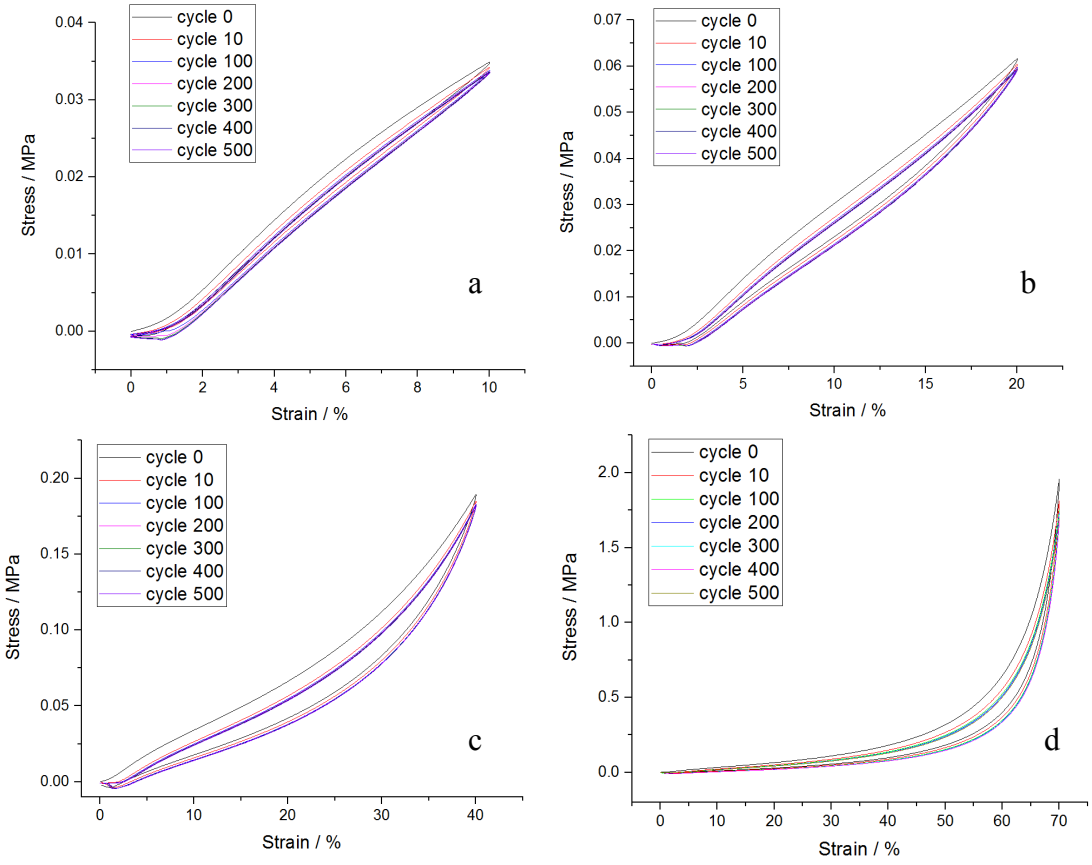

Appendix III **Shear-dependent viscosity data for H/MIPEs. Lines illustrate data fitting to the Carreau–Yasuda model. Temperature = 25 °C.**

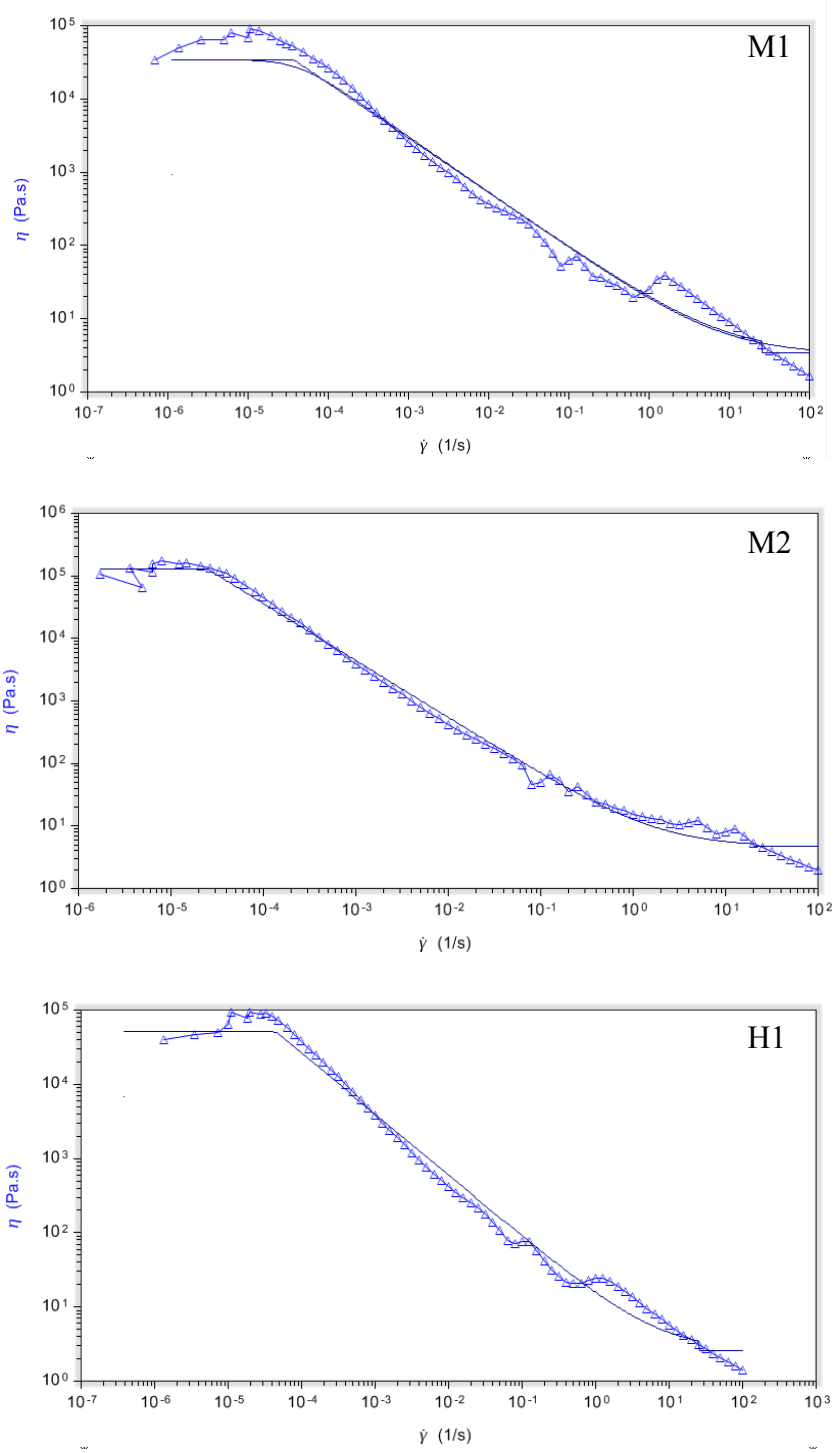

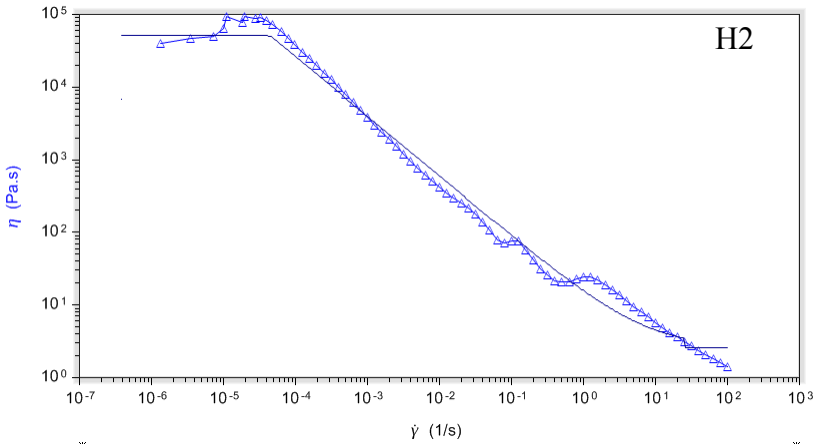

Appendix IV **The SEM images of the cross sections of screen printed PM2 with different mesh size screens.**

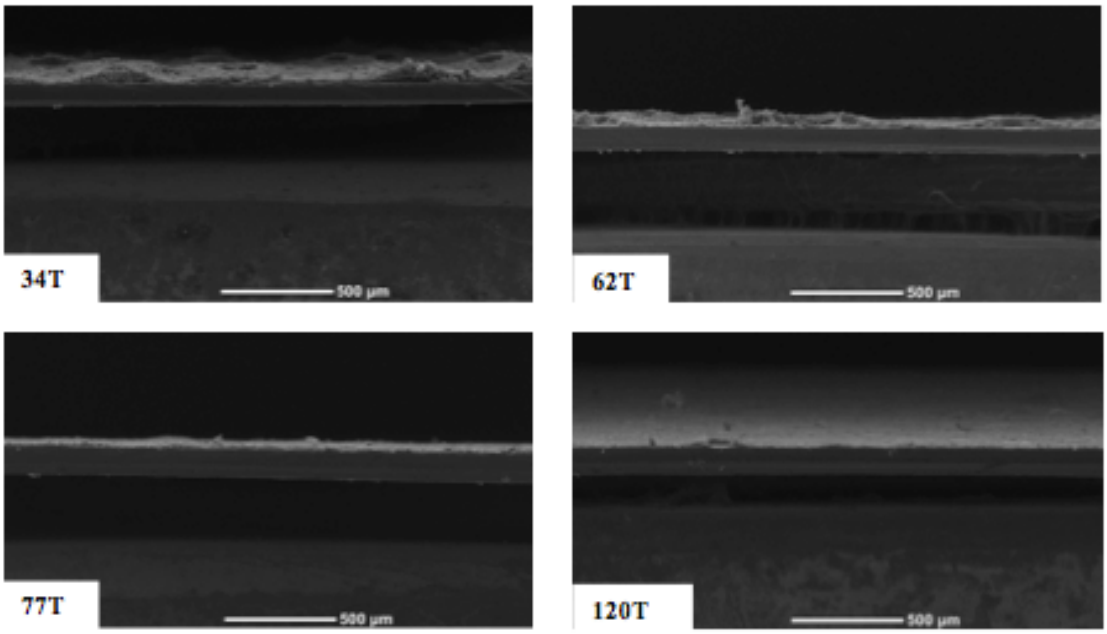

Appendix V **The cage patterns of PH3 with different coordinates printed with syringe printer using 0.7 mm outer diameter needle.**